A 12 GeV Research Proposal to Jefferson Lab (PAC 39)

# Measurement of transversity with dihadron production in SIDIS with transversely polarized target


H. Avakian[†*], V.D. Burkert, L. Elouadrhiri, T. Kageya, V. Kubarovsky
M. Lowry, A. Prokudin, A. Puckett, A. Sandorfi, Yu. Sharabian, X. Wei
Jefferson Lab, Newport News, VA 23606, USA

S. Anefalos Pereira[†], M. Aghasyan, E. De Sanctis, D. Hasch, L. Hovsepyan,
V. Lucherini, M. Mirazita, S. Pisano, and P. Rossi
INFN, Laboratori Nazionali di Frascati , Frascati, Italy

A. Courtoy[†]
IFPA-Institut de Physique Universite de Liege (ULg), Allee du 6 Aout 17, bat. B5 4000 Liege, Belgium

A. Bacchetta, M. Radici[†], B. Pasquini
Universita' di Pavia and INFN Sezione di Pavia, via Bassi 6, 27100 Pavia, Italy

L. Pappalardo[†], L. Barion, G. Ciullo, M. Contalbrigo, P.F. Dalpiaz,P. Lenisa, M. Statera
University of Ferrara and INFN Ferrara, Via Saragat, I-44100, Ferrara, Italy

K. Griffioen[†]
College of William & Mary, VA 23187, USA

G. Schnell
The University of the Basque Country, Postal 644, E-48080 Bilbao, Spain

K. Joo, P. Schweitzer,
University of Connecticut, Storrs, CT 06269, USA

G. De Cataldo, R. De Leo, L. La Gamba, E. Nappi, R. Perrino
University of Bari and INFN Bari, Via Orabona, I-70125, Bari, Italy

M. Battaglieri, A. Celentano, R. De Vita, M. Osipenko, M. Ripani, M. Taiuti
Dipartamento di Fisica and INFN, Sezione di Genova, Via Dodecaneso, 33 I-16146 Genova, Italy

V. Bellini, A. Giusa, F. Mammoliti, F. Noto, G. Russo, L. Sperduto, C. Sutera
University of Catania and INFN Catania, Via S. Sofia, I-95123 Catania, Italy

A. D'Angelo, C. Schaerf, I. Zonta
Dipartimento di Fisica, Universita' di Roma Tor Vergata,
INFN Sezione di Roma Tor Vergata, Via della Ricerca Scientifica, I-00133, Rome, Italy

F. Meddi, G.M. Urciuoli
INFN Roma I, P.le aldo Moro, I-00185, Roma, Italy

E. Cisbani, A. Del Dotto, F. Garibaldi, S. Frullani
INFN Roma I and Istituto Superiore di Sanita', Viale Regina Elena, I-00161, Roma, Italy

M. Capogni
INFN Roma I and ENEA Casaccia, Via Anguillarese, I-00123, Roma, Italy

M. Anselmino, A. Kotzinian, B. Parsamyan
Università di Torino and INFN, Sezione di Torino, Via P. Giuria 1, I-10125 Torino

A CLAS collaboration proposal

† Co-spokesperson * Contact: Harut Avakian, JLab,Newport News VA 23606. Email: avakian@jlab.org

**Abstract**

We propose to study the target spin asymmetries in dihadron production in semi-inclusive DIS (SIDIS) using an 11 GeV electron beam from the upgraded CEBAF facility and the CLAS12 detector equipped with a transversely polarized target. The main focus of the experiment will be the measurement of leading twist transversity distribution in the reaction $ep^{\uparrow} \rightarrow e\pi^{+}\pi^{-}X$ . The transversity distribution, $h_1$, which describes transversely polarized quarks in the transversely polarized nucleon is the least known of the three fundamental collinear PDFs of the nucleon. The transversity distribution and its first moment, the tensor charge, are as fundamental for understanding of the spin structure of the nucleon as are the helicity distribution $g_1$ and the axial vector charge. Unlike $g_1$, $h_1$ is chirally odd, i.e. it requires a quark helicity flip that cannot be achieved in inclusive DIS and pion pair production provides a unique model independent procedure for extracting it in electroproduction.

The expected asymmetries from the leading-order calculations and Monte Carlo studies are in the range of 2 to 10%, depending on the kinematics and on the models used for the transversity PDF. The $x$, $Q^2$, $z$ and $M_{\pi\pi}$ dependences of the target spin asymmetries will be studied over a wide kinematic range.
A total of 110 days of beam time is requested for this experiment.

# Contents

# 1 Introduction

The distribution of quarks and gluons inside hadrons can be described by means of parton distribution functions (PDFs). In a parton-model picture, PDFs describe combinations of number densities of quarks and gluons in a fast-moving hadron. The knowledge of PDFs is crucial for our understanding of Quantum Chromodynamics (QCD) and for the interpretation of high-energy experiments involving hadrons.

In the Bjorken limit the partonic structure of the nucleon is described by three PDFs: the well known unpolarized, $f_1^q(x)$, and helicity, $g_1^q(x)$, distribution functions, and the transversity distribution function $h_1^q(x)$, which measures the transverse polarization of quarks with flavor $q$ and fractional momentum $x$ in a transversely polarized nucleon [1, 2, 3]. Intuitively, helicity and transversity give two orthogonal pictures of the partonic structure of polarized nucleons. They have very different properties, and transversity is poorly known. We propose here to study a target spin asymmetry in dihadron production that can be used to extract the transversity distribution, using an 11 GeV electron beam from the upgraded CEBAF facility and the CLAS12 detector equipped with a transversely polarized target.

Transversity arises from the interference of amplitudes with different parton and parent nucleon helicities. In jargon, it is called a chiral-odd function. There is no transversity for gluons in a nucleon, and $h_1^q$ evolves with $Q^2$ as a pure non-singlet [4]. From transversity one can build the nucleon tensor charge, which is odd under charge conjugation and can be computed in lattice QCD [5] (for a review on transversity, see Ref. [6] and references therein).

Transversity is particularly difficult to measure because it must appear in cross sections combined with another chiral-odd function. The simplest example is the cross section of the transversely polarized Drell-Yan process, where $h_1^q$ appears multiplied by its antiquark partner $h_1^{\bar{q}}$ [1, 3]. At present, there exists no measurement of this process.

Another example is the cross section for single-particle inclusive Deep Inelastic Scattering (DIS),

$$\ell(l) + N(P) \to \ell(l') + H(P_h) + X \quad ,$$

where $h_1^q$ appears in a convolution with the chiral-odd Collins fragmentation function $H_1^{\perp q}$ [7], which describes the correlation between the transverse polarization of a fragmenting quark with flavor $q$ and the transverse momentum distribution of the detected unpolarized hadron. It is a non-collinear fragmentation function, which allows for azimuthal hadron asymmetries that depend on the transverse hadron momentum $P_{h\perp}$. One is hence forced to account for the transverse momentum $k_\perp$ of quarks as well. This leads to the convolution $h_1^q \otimes H_1^{\perp\, q}$ that gives rise to a specific azimuthal modulation of the cross section. The amplitude of the modulation has been measured by the HERMES and COMPASS collaborations [8, 9]. In order to extract the transversity distribution from this signal, the Collins function should be determined through the measurement of azimuthal asymmetries in the distribution of two almost

back-to-back hadrons in $e^+e^-$ annihilation [10]. The Belle collaboration has measured this asymmetry [11, 12], making the first-ever extraction of $h_1^q$ possible from a simultaneous analysis of $ep^\uparrow \to e'\pi X$ and $e^+e^- \to \pi\pi X$ data [13]. The transversity accessed through this process is encapsulated in the Transverse Momentum Distribution (TMD) $h_1(x, k_\perp, Q^2)$.

In spite of this breakthrough, some questions still hinder the extraction of transversity from single-particle-inclusive measurements. A most crucial issue is the treatment of $Q^2$-evolution, since the measurements were performed at very different energies. The convolution $h_1^q \otimes H_1^{\perp\, q}$ involves the transverse momentum of quarks. Hence, its evolution should be described in the framework of the transverse-momentum-dependent factorization [14, 15]. Quantitative estimates suggest that neglecting evolution effects could lead to overestimating transversity [16, 17]. The so-called TMD framework has been extensively studied (e.g. Bessel weighting treatment of cross sections [18]) but it is only recently that the TMD evolution has been addressed [19].

In this context, it is of paramount importance to extract transversity in an independent way, requiring only standard collinear factorization where the above complications are absent (see, e.g, Refs. [20, 21] and references therein). In this context, we propose to study the semi-inclusive deep-inelastic production of two pions with small invariant mass,

$$\ell(l) + N(P) \to \ell(l') + H_1(P_1) + H_2(P_2) + X \quad .$$

In this case, the transversity distribution function is combined with a chiral-odd Dihadron Fragmentation Function (DiFF), denoted as $H_1^{\sphericalangle\, q}$ [22], which describes the correlation between the transverse polarization of the fragmenting quark with flavor $q$ and the azimuthal orientation of the plane containing the momenta of the detected hadron pair. Contrary to the Collins mechanism, this effect survives after integration over quark transverse momenta and can be analyzed in the framework of collinear factorization. This process has been studied from different perspectives in a number of papers [23, 24, 25, 22, 26].

There are at present only two published measurements of the relevant asymmetry, one by the HERMES collaboration for the production of $\pi^+\pi^-$ pairs on transversely polarized protons [27], and the other by the COMPASS collaboration for the production of unidentified $H^+H^-$ pairs on transversely polarized protons and deuterons [28]. Combined with the Belle data on the Artru–Collins azimuthal asymmetry [29], i.e. azimuthal orientations of two pion pairs in back-to-back jets in $e^+e^-$ annihilation [30, 31], those data have made possible the first extraction of transversity in a collinear framework [32], where factorization and evolution are both well understood. In other words, transversity as accessed through dihadron production is a collinear PDF $h_1(x, Q^2)$, i.e. with no transverse-momentum dependence.

Despite all these developments, transversity data are still scarce compared to the data for $f_1$ and $g_1$. For the Collins asymmetry in single-hadron production, there are

about 100 points in $x$, including the recent neutron data from Hall A on a transversely polarized $^3$He target [33]. At present, the total set of dihadron data is limited to about 20 points in $x$ within the range $x \in [0.005, 0.3]$. The available COMPASS results come from data taken in the 2002-2004 run on a $^6$LiD deuteron target, and from the 2007 run on a $NH_3$ proton target [28]. The collaboration is analyzing new data collected in the 2010 run on a proton target. Related unidentified pair production in proton-proton scattering has been presented by the PHENIX collaboration for the 2006-2008 run at mid-rapidity and center-of-mass energy $\sqrt{s} = 200$ GeV [34]. The total amount of data is an order of magnitude less than for the extraction of $g_1$ (see, e.g., Ref. [35]).

As will be shown in the present proposal, CLAS12 offers the possibility of exploring a wider kinematical range, especially in $x$, for dihadron production in SIDIS, which will significantly improve the determination of transversity.

# 2 Theoretical framework

We consider the process

$$\ell(l) + N(P) \to \ell(l') + H_1(P_1) + H_2(P_2) + X, \tag{1}$$

where $\ell$ denotes the beam lepton, $N$ the nucleon target, $H_1$ and $H_2$ the produced hadrons, and where four-momenta are given in parentheses. We work in the one-photon exchange approximation and neglect the lepton mass. We denote by $M$ the mass of the nucleon and by $S$ its polarization. The final hadrons, with mass $M_1$, $M_2$ and momenta $P_1$, $P_2$, have invariant mass $M_h$(which we consider much smaller than the hard scale $Q^2 = -q^2 \geq 0$ of the SIDIS process). We introduce the pair total momentum $P_h = P_1 + P_2$ and relative momentum $R = (P_1 - P_2)/2$.

As usual we define $q = l - l'$ and introduce the variables

$$x = \frac{Q^2}{2\,P\cdot q}, \qquad y = \frac{P\cdot q}{P\cdot l}, \qquad z = \frac{P\cdot P_h}{P\cdot q}, \qquad \gamma = \frac{2Mx}{Q}. \tag{2}$$

In the center-of-mass (cm) frame of the two hadrons, the emission occurs back-to-back and the key variable is the polar angle $\theta$ between the directions of the emission and the direction of $P_h$ in the photon-proton center-of-mass frame.

Finally, the azimuthal angles are defined as in Fig. 1 [27].[1]

To leading-order, the cross section for two-particle inclusive DIS can be written

[1] From the theoretical point of view, different definitions for the azimuthal angles may be adopted, as long as they differ by terms of order $\gamma^2$.

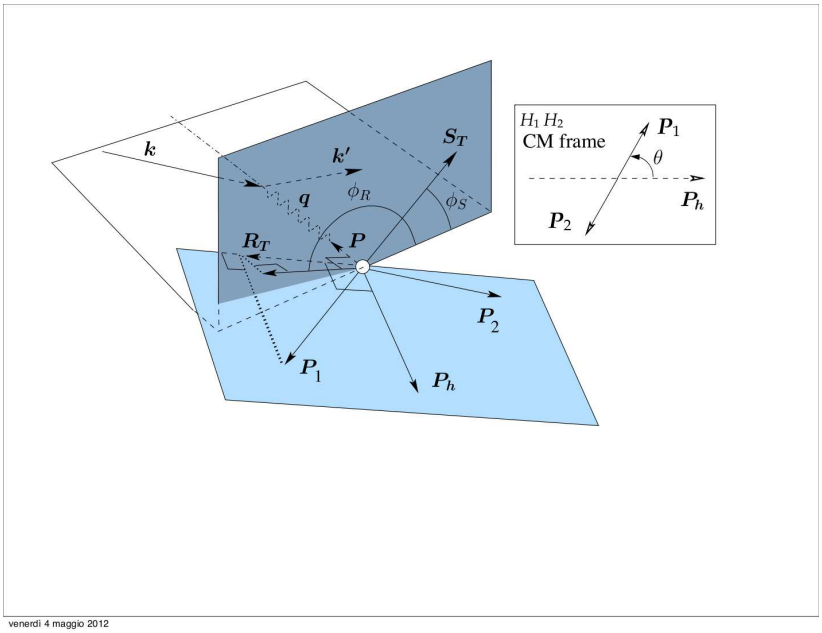


Figure 1: Depiction of the azimuthal angles $\phi_R$ of the dihadron and $\phi_S$ of the component $\boldsymbol{S}_T$ of the target-polarization transverse to both the virtual-photon and target-nucleon momenta $\boldsymbol{q}$ and $\boldsymbol{P}$, respectively. Both angles are evaluated in the virtual-photon-nucleon center-of-momentum frame. Here, $\boldsymbol{R}_T = \boldsymbol{R} - (\boldsymbol{R}\cdot\hat{\boldsymbol{P}}_h)\hat{\boldsymbol{P}}_h$, i.e., $R_T$ is the component of $P_1$ orthogonal to $P_h$; up to subleading-twist corrections, it can be identified with its projection to the plane perpendicular to $\boldsymbol{q}$ that contains $\boldsymbol{S}_T$. Thus, the angle $\phi_R$ is the azimuthal angle of $R_T$ about the virtual-photon direction. Explicitly, $\phi_R \equiv \frac{(\boldsymbol{q}\times\boldsymbol{k})\cdot\boldsymbol{R}_T}{|(\boldsymbol{q}\times\boldsymbol{k})\cdot\boldsymbol{R}_T|}\arccos\frac{(\boldsymbol{q}\times\boldsymbol{k})\cdot(\boldsymbol{q}\times\boldsymbol{R}_T)}{|\boldsymbol{q}\times\boldsymbol{k}||\boldsymbol{q}\times\boldsymbol{R}_T|}$ and $\phi_S \equiv \frac{(\boldsymbol{q}\times\boldsymbol{k})\cdot\boldsymbol{S}_T}{|(\boldsymbol{q}\times\boldsymbol{k})\cdot\boldsymbol{S}_T|}\arccos\frac{(\boldsymbol{q}\times\boldsymbol{k})\cdot(\boldsymbol{q}\times\boldsymbol{S}_T)}{|\boldsymbol{q}\times\boldsymbol{k}||\boldsymbol{q}\times\boldsymbol{S}_T|}$. Also included is a description of the polar angle $\theta$, which is evaluated in the center-of-momentum frame of the pion pair.

as [36]

$$
\begin{aligned}
&\frac{d\sigma}{dx\,dy\,d\psi\,dz\,d\phi_R\,dM_h^2\,d\cos\theta} = \\
&\quad\frac{\alpha^2}{xy\,Q^2}\,\frac{y^2}{2\,(1-\varepsilon)}\left(1+\frac{\gamma^2}{2x}\right)\Bigg\{F_{UU,T} + \varepsilon\,F_{UU,L} + \sqrt{2\,\varepsilon(1+\varepsilon)}\,\cos\phi_R\,F_{UU}^{\cos\phi_R} \\
&\qquad + \varepsilon\cos(2\phi_R)\,F_{UU}^{\cos 2\phi_R} + \lambda_e\,\sqrt{2\,\varepsilon(1-\varepsilon)}\,\sin\phi_R\,F_{LU}^{\sin\phi_R} \\
&\qquad + S_L\left[\sqrt{2\,\varepsilon(1+\varepsilon)}\,\sin\phi_R\,F_{UL}^{\sin\phi_R} + \varepsilon\sin(2\phi_R)\,F_{UL}^{\sin 2\phi_R}\right] \\
&\qquad + S_L\lambda_e\left[\sqrt{1-\varepsilon^2}\,F_{LL} + \sqrt{2\,\varepsilon(1-\varepsilon)}\,\cos\phi_R\,F_{LL}^{\cos\phi_R}\right] \\
&\qquad + |\boldsymbol{S}_T|\Bigg[\sin(\phi_R-\phi_S)\left(F_{UT,T}^{\sin(\phi_R-\phi_S)} + \varepsilon\,F_{UT,L}^{\sin(\phi_R-\phi_S)}\right) \\
&\qquad\quad + \varepsilon\,\sin(\phi_R+\phi_S)\,F_{UT}^{\sin(\phi_R+\phi_S)} + \varepsilon\,\sin(3\phi_R-\phi_S)\,F_{UT}^{\sin(3\phi_R-\phi_S)} \\
&\qquad\quad + \sqrt{2\,\varepsilon(1+\varepsilon)}\,\sin\phi_S\,F_{UT}^{\sin\phi_S} + \sqrt{2\,\varepsilon(1+\varepsilon)}\,\sin(2\phi_R-\phi_S)\,F_{UT}^{\sin(2\phi_R-\phi_S)}\Bigg]
\end{aligned}
$$

where $\alpha$ is the fine structure constant, $\lambda_e$ is the beam longitudinal polarization, and the structure functions on the r.h.s. depend on $x$, $Q^2$, $z$, $\cos\theta$, ans $M_h^2$. The angle $\psi$ is the azimuthal angle of $\ell'$ around the lepton beam axis with respect to an arbitrary fixed direction, which in case of a transversely polarized target we choose to be the direction of $S$. The corresponding relation between $\psi$ and $\phi_S$ is given in Ref. [37]; in deep inelastic kinematics one has $d\psi \approx d\phi_S$. The first and second subscripts of the above structure functions indicate the respective polarization of beam and target, whereas the third subscript in $F_{UU,T}$, $F_{UU,L}$ and $F_{UT,T}^{\sin(\phi_h-\phi_S)}$, $F_{UT,L}^{\sin(\phi_h-\phi_S)}$ specifies the polarization of the virtual photon. Note that here longitudinal or transverse target polarizations refer to the photon direction. The conversion to the experimentally relevant longitudinal or transverse polarization w.r.t. the lepton beam direction is straightforward and given in [37].

The ratio $\varepsilon$ of longitudinal and transverse photon flux in (3) is given by [36]

$$\varepsilon = \frac{1 - y - \frac{1}{4}\gamma^2 y^2}{1 - y + \frac{1}{2}y^2 + \frac{1}{4}\gamma^2 y^2}, \tag{4}$$

so that the depolarization factors can be written as

$$\frac{y^2}{2\,(1-\varepsilon)} = \frac{1}{1+\gamma^2}\left(1 - y + \tfrac{1}{2}y^2 + \tfrac{1}{4}\gamma^2 y^2\right) \approx \left(1 - y + \tfrac{1}{2}y^2\right) \equiv A(y) \quad , \tag{5}$$

$$\frac{y^2}{2\,(1-\varepsilon)}\,\varepsilon = \frac{1}{1+\gamma^2}\left(1 - y - \tfrac{1}{4}\gamma^2 y^2\right) \approx (1-y) \equiv B(y) \quad , \tag{6}$$

$$\frac{y^2}{2\,(1-\varepsilon)}\,\sqrt{2\,\varepsilon(1+\varepsilon)} = \frac{1}{1+\gamma^2}\,(2-y)\,\sqrt{1 - y - \tfrac{1}{4}\gamma^2 y^2} \approx (2-y)\,\sqrt{1-y} \equiv V(y) \quad , \tag{7}$$

$$\frac{y^2}{2\,(1-\varepsilon)}\,\sqrt{2\,\varepsilon(1-\varepsilon)} = \frac{1}{\sqrt{1+\gamma^2}}\,y\,\sqrt{1 - y - \tfrac{1}{4}\gamma^2 y^2} \approx y\,\sqrt{1-y} \equiv W(y) \quad , \tag{8}$$

$$\frac{y^2}{2\,(1-\varepsilon)}\,\sqrt{1-\varepsilon^2} = \frac{1}{\sqrt{1+\gamma^2}}\,y\left(1 - \tfrac{1}{2}y\right) \approx y\left(1 - \tfrac{1}{2}y\right) \equiv C(y) \quad . \tag{9}$$

The relevant spin asymmetries can be built as ratios of structure functions. Different choices and definitions are possible. Here we try to be consistent with the past literature [27] and the Trento conventions [38].

For an unpolarized beam and a transversely polarized target, i.e. for the $UT$

combination, one can define the following asymmetry:

$$A_{UT}^{\sin(\phi_R+\phi_S)\,\sin\theta}(x,y,z,M_h,Q) = \frac{1}{|\boldsymbol{S}_T|}\,\frac{\frac{8}{\pi}\int d\phi_R\, d\cos\theta\,\sin(\phi_R+\phi_S)\,(d\sigma^{\uparrow}-d\sigma^{\downarrow})}{\int d\phi_R\, d\cos\theta\,(d\sigma^{\uparrow}+d\sigma^{\downarrow})}$$
$$= \frac{\frac{4}{\pi}\,\varepsilon\int d\cos\theta\,F_{UT}^{\sin(\phi_R+\phi_S)}}{\int d\cos\theta\,(F_{UU,T}+\varepsilon\,F_{UU,L})} \quad . \tag{10}$$

We note that the above definitions assume a full integration over $\phi_R$ and $\cos\theta$.

In the limit[2] $M_h^2 \ll Q^2$ the structure functions can be written in terms of PDFs and DiFFs as follows with the summation $\sum_q e_q^2$ understood [40]

$$F_{UU,T} = x f_1(x)\, D_1\big(z,\cos\theta,M_h\big), \tag{11}$$

$$F_{UU,L} = 0, \tag{12}$$

$$F_{UU}^{\cos\phi_R} = -x\frac{|\boldsymbol{R}|\sin\theta}{Q}\,\frac{1}{z}\,f_1(x)\,\widetilde{D}^{\sphericalangle}\big(z,\cos\theta,M_h\big), \tag{13}$$

$$F_{UU}^{\cos 2\phi_R} = 0, \tag{14}$$

$$F_{UT,T}^{\sin(\phi_R-\phi_S)} = 0, \tag{15}$$

$$F_{UT,L}^{\sin(\phi_R-\phi_S)} = 0, \tag{16}$$

$$F_{UT}^{\sin(\phi_R+\phi_S)} = x\frac{|\boldsymbol{R}|\sin\theta}{M_h}\,h_1(x)\,H_1^{\sphericalangle}\big(z,\cos\theta,M_h^2\big), \tag{17}$$

$$F_{UT}^{\sin(3\phi_R-\phi_S)} = 0, \tag{18}$$

$$F_{UT}^{\sin\phi_S} = x\frac{M_h}{Q}\left[h_1(x)\left(\frac{1}{z}\,\widetilde{H}\big(z,\cos\theta,M_h^2\big) + \frac{|\boldsymbol{R}|^2\sin\theta^2}{M_h^2}\,H_1^{\sphericalangle\,o\,(1)}\big(z,\cos\theta,M_h^2\big)\right)\right.$$
$$\left. - \frac{M}{M_h}\,x\,f_T(x)\,D_1\big(z,\cos\theta,M_h^2\big)\right], \tag{19}$$

$$F_{UT}^{\sin(2\phi_R-\phi_S)} = 0, \tag{20}$$

$$F_{LT}^{\cos(\phi_R-\phi_S)} = 0, \tag{21}$$

$$F_{LT}^{\cos\phi_R} = \frac{M_h}{Q}\left[-\frac{M}{M_h}\,x\,g_T(x)\,D_1\big(z,\cos\theta,M_h^2\big) - \frac{1}{z}\,h_1(x)\,\widetilde{E}\big(z,\cos\theta,M_h^2\big)\right], \tag{22}$$

$$F_{LT}^{\cos(2\phi_R-\phi_S)} = 0. \tag{23}$$

[2]For some discussion of the case $M_h^2 \approx Q^2$, see Ref. [39]

To be more concise, we have used the definition

$$|\boldsymbol{R}| = \frac{1}{2}\sqrt{M_h^2 - 2(M_1^2 + M_2^2) + (M_1^2 - M_2^2)^2}\ . \tag{24}$$

All the structure functions that vanish can be nonzero at order $\mathcal{O}\Big(\frac{M^2}{Q^2}, \frac{M_h^2}{Q^2}\Big)$. The higher-twist DiFFs are defined in Ref. [40]. In the present proposal, we focus on the leading-twist effects. Hence, the most interesting term for our purposes is the structure function containing the PDF $h_1$, multiplied by the interference fragmentation function $H_1^{\sphericalangle}$, occurring in the structure functions $F_{UT}^{\sin(\phi_R+\phi_S)}$ of Eq. (17). The higher-twist effects, in particular the structure function Eq. (19), will be studied as source of systematic errors.

The extraction of the transversity PDF is made possible by the fact that $H_1^{\sphericalangle}$ has been recently extracted [41] from Belle measurements [29] (see the next Section).

## 2.1 The dihadron fragmentation functions (DiFFs)

Two-hadron fragmentation functions can be decomposed into partial waves in the following way [26]:

$$D_1 \to D_{1,ss+pp} + D_{1,sp}\cos\theta + D_{1,pp}\frac{1}{4}\left(3\cos^2\theta - 1\right)\ , \tag{25}$$

$$H_1^{\sphericalangle} \to H_{1,sp}^{\sphericalangle} + H_{1,pp}^{\sphericalangle}\cos\theta\ , \tag{26}$$

where the relative partial waves of each pion pair are made evident. The notation $ss+pp$ refers to hadron pairs created with a relative $\Delta L = 0$, i.e. unpolarized ; while the $sp$ refers the interference between pion pairs in $s$ and $p$ waves with a relative $\Delta L = 1$. For simplicity, we will use the notation $D_{1,ss+pp} \equiv D_1$ since no ambiguity arises in the following. The functions $\widetilde{H}$ and $\widetilde{E}$ can be expanded in the same way as $D_1$, and the function $\widetilde{D}^{\sphericalangle}$ in the same way as $H_1^{\sphericalangle}$. The functions on the r.h.s. depend on $z$ and $M_h$. It may be useful to note that a symmetrization $f(\theta) + f(\pi - \theta)$ gets rid of all the $\cos\theta$ terms [27]. In general, those terms will vanish even if the $\theta$ acceptance is not complete but still symmetric about $\theta = \pi/2$.

A thorough study of the cross section with a partial-wave analysis has been recently presented in Ref. [42], with a different notation compared to the one adopted here.

We now make a flavor analysis of the structure functions. The analysis will be different depending on the kind of target and final-state hadrons. We will consider here only proton or deuteron targets and $\pi^+\pi^-$ final-state pairs.

Isospin symmetry and charge conjugation suggest the relations [32]

$$D_1^{u\to\pi^+\pi^-} = D_1^{d\to\pi^+\pi^-} = D_1^{\bar{u}\to\pi^+\pi^-} = D_1^{\bar{d}\to\pi^+\pi^-} \,, \tag{27}$$

$$D_1^{s\to\pi^+\pi^-} = D_1^{\bar{s}\to\pi^+\pi^-} \,, \tag{28}$$

$$D_1^{c\to\pi^+\pi^-} = D_1^{\bar{c}\to\pi^+\pi^-} \,, \tag{29}$$

$$H_1^{\sphericalangle u\to\pi^+\pi^-} = -H_1^{\sphericalangle d\to\pi^+\pi^-} = -H_1^{\sphericalangle \bar{u}\to\pi^+\pi^-} = H_1^{\sphericalangle \bar{d}\to\pi^+\pi^-} \,, \tag{30}$$

$$H_1^{\sphericalangle s\to\pi^+\pi^-} = -H_1^{\sphericalangle \bar{s}\to\pi^+\pi^-} = H_1^{\sphericalangle c\to\pi^+\pi^-} = -H_1^{\sphericalangle \bar{c}\to\pi^+\pi^-} = 0 \,. \tag{31}$$

In practice, for $\pi^+\pi^-$, there are only three independent $D_1$ functions and one $H_1^{\sphericalangle}$ function.

Before the Belle measurement of the angular distribution of two pion pairs in $e^+e^-$ annihilation [29], the only estimates of DiFFs were based on model calculations [43, 22, 44]. The unpolarized $D_1$ was tuned to Monte Carlo event generators [44] and the polarized $H_{1,sp}^{\sphericalangle}$ compared to HERMES asymmetry data [45]. Recently the DiFF $D_1$ was also calculated in the NJL-jet model [46].

The first analysis [29] of the so-called Artru–Collins asymmetry [47] by the Belle collaboration made possible a direct extraction of $H_{1,sp}^{\sphericalangle}$ for the production of $\pi^+\pi^-$.

In the absence of a measurement of the unpolarized cross section for dihadron production in $e^+e^-$ annihilation (planned at Belle in the near future), $D_1$ was parametrized to reproduce the two-hadron yields of the PYTHIA event generator, which is known to give a good description of data. Four main decay channels were considered for $\pi^+\pi^-$: (i) $\rho$ resonance decaying into the two pions, (ii) $\omega$ resonance decaying into the two pions, plus the fragmentation into a $\omega$ resonance decaying into $\pi^+\pi^-\pi^0$ with $\pi^0$ unobserved, (iii) $K_S^0$ resonance decaying into $(\pi^+\pi^-)$, (iv) the continuum ( *i.e.* the fragmentation into an "incoherent" $\pi^+\pi^-$ pair). Combining the parametrization of the unpolarized functions $D_1$ with the fit of the azimuthal asymmetry presented in Ref. [29], it was possible to extract the DiFF $H_{1,sp}^{\sphericalangle}$ [41].

In Fig. 2, we show the ratio

$$R(z, M_{\pi\pi}) = \frac{|\boldsymbol{R}|}{M_{\pi\pi}} \frac{H_{1,sp}^{\sphericalangle u}(z, M_{\pi\pi}; Q_0^2)}{D_1^u(z, M_{\pi\pi}; Q_0^2)} \,, \tag{32}$$

summed over all channels, at the hadronic scale $Q_0^2 = 1$ GeV$^2$. The errors are estimated through the propagation from the fit.

Evolution effects affect both $D_1$ and $H_1^{\sphericalangle}$ separately, but the $Q^2$-dependence is found to cancel to a large extent when taking the ratio $H_1^{\sphericalangle}/D_1$ in the asymmetry [45]. Therefore, $Q^2$ evolution is insignificant in comparison with other uncertainties in the calculation, and for the present proposal, we will assume no $Q^2$-dependence.

For the purposes of extracting the transversity distribution, the most relevant

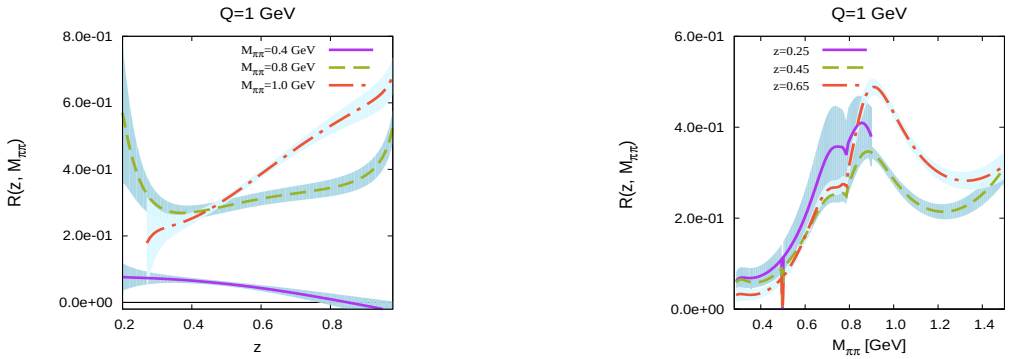


Figure 2: The ratio $R(z,M_{\pi\pi})$ of Eq. (32) as a function of $z$ and $M_{\pi\pi}$ respectively. The error bars come from the calculation of error propagation from the fit.

quantities are the integrals

$$\begin{aligned} n_q(Q^2) &= \int dz\, dM_{\pi\pi}\, D_1^q(z, M_{\pi\pi}; Q^2) \\ n_q^{\uparrow}(Q^2) &= \int dz\, dM_{\pi\pi}\, \frac{|\boldsymbol{R}|}{M_{\pi\pi}}\, H_{1,sp}^{\sphericalangle q}(z, M_{\pi\pi}; Q^2)\ . \end{aligned} \tag{33}$$

## 2.2 The transversity distribution function

A comprehensive review of the properties of the transversity distribution function can be found in Ref. [6]. Transversity $h_1$, as leading-twist collinear PDF, enjoys the same status as $f_1$ and $g_1$ [1, 48]. The distribution of transversely polarized quarks $q^{\uparrow}$ in a transversely polarized nucleon $p^{\uparrow}$ (integrated over transverse momentum) can be written as[3]

$$f_{q^{\uparrow}/p^{\uparrow}}(x) = f_1^q(x) + \boldsymbol{S}\cdot\boldsymbol{S}_q\, h_1^q(x) \quad , \tag{34}$$

in which $\boldsymbol{S}$ is the nucleon spin and $\boldsymbol{S}_q$ the quark spin. Therefore, transversity can be interpreted as the difference between the probability of finding a parton (with flavor $q$ and momentum fraction $x$) with transverse spin parallel and anti-parallel to that of the transversely polarized nucleon.

In a non-relativistic framework $h_1 = g_1$, since rotations in spin space between different bases commute with spatial operations (like Euclidean boosts), but relativistically $h_1$ and $g_1$ are different. Therefore any difference between helicity and transversity PDFs is related to the relativistic nature of parton dynamics inside hadrons. Moreover, since perturbative QCD preserves chirality in the massless limit, transversity is related to nonperturbative QCD effects such as chiral symmetry breaking and mass generation [49].

[3]We remark that, of the four-dimensional Dirac space of quarks, only a two-dimensional subspace ("good quarks") is relevant at leading twist. This is important to avoid confusions with the subleading-twist distribution $g_T$.

An important difference between $h_1$ and $g_1$ is that in spin-$\frac{1}{2}$ hadrons there is no gluonic function analogous to transversity. The most important consequence is that $h_1^q$ for a quark with flavor $q$ does not mix with gluons in its evolution and it behaves as a non-singlet quantity; this has been verified up to NLO, where chiral-odd evolution kernels have been studied so far [50, 51, 52].

The tensor charge of the nucleon is defined as the sum of the Mellin moments

$$\delta_T q(Q^2) = \int dx \left[ h_1^q(x, Q^2) - h_1^{\bar{q}}(x, Q^2) \right] \quad . \tag{35}$$

Contrary to the axial charge — which is related to $g_1^q(x, Q^2)$ — it has a non-vanishing anomalous dimension and therefore evolves with the hard scale $Q^2$ [48]. It has been calculated on the lattice [5] and in various models [53, 54, 55, 56, 57], and it turns out not to be small. While the axial charge is a charge-even operator, from Equation (35) it is evident that the tensor charge is odd under charge conjugation and, therefore, it does not receive contributions from $q\bar{q}$ pairs in the sea and is dominated by valence contributions. This feature, and the typical non-singlet evolution, suggest that transversity is one of the best tools to explore the valence part of the partonic content of the nucleon. In Fig. 3, we show some estimates of the tensor charge for up and down quarks separately, together with the combined results of transversity extraction (red triangles). The error band on the tensor charges calculated from the extraction [58] are certainly underestimated, since they do not take into account the errors due to the extrapolation outside the $x$-range where data are presently available.

Because a probability must be positive, we get the important Soffer inequality [59],

$$2|h_1^q(x, Q^2)| \leq f_1^q(x, Q^2) + g_1^q(x, Q^2) \ , \tag{36}$$

which is true at all $Q^2$ [60, 52]. An analogous relation holds for antiquark distributions. All of the models, including the lattice predictions, find a positive tensor charge for the $u$-quark and a negative one for the $d$-quark. There are no data so far to verify this inequality.

Ref. [6] lists various classes of models for the transversity distribution including bag-like models, e.g. [2]; chiral quark soliton models, e.g. [61]; light-cone models, e.g. [62]; and diquark spectator models, e.g. [63]. A comparison of the models results shows that, at low momentum scales, $h_1$ is not so different from $g_1$, at least for the dominant $u$ sector. It would therefore be interesting to explore this more deeply by gathering more experimental data.

In Fig. 4, we show several model calculations of transversity compared to the presently available parametrization of Ref. [58]. The central value of the present extraction for up quarks is systematically lower than most model calculations, while the central value of the extraction for down quarks tends to be similar. All model calculations are affected by an uncertainty related to the choice of the hadronic scale where DGLAP evolution is switched on. Two important remarks are in order: first,

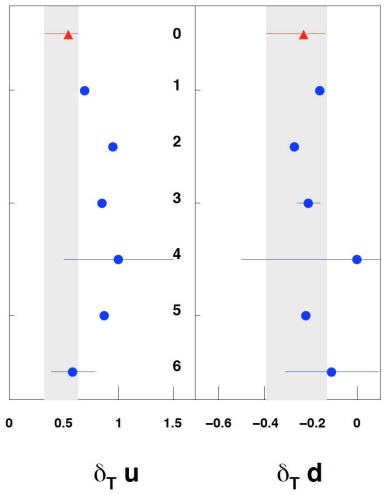


Figure 3: Tensor charge from: (0) the fit to data [58], (1) the quark-diquark model [53], (2) the chiral quark-soliton model [54], (3) lattice QCD [5], (4) QCD sum rules [55], (5) the constituent quark model [56], and (6) spin-flavour SU(6) symmetry [57]. The error band corresponds to the errors from the fit [58]. This figure is from Ref. [58].

no data exist for $x > 0.4$; secondly, the *sign* of the up quark distribution cannot be determined from experimental measurements.

In this proposal, we have considered three estimates for $h_1(x)$: the Light-Cone Constituent Quark Model prediction(LCCQM) [56], the diquark spectator model prediction [68] and the extraction of Ref. [58]. They are all shown in Fig. 5.

# 3 Asymmetries and predictions

Using the expressions of the structure functions Eqs. (12)–(23), dropping corrections of order $M/Q$, and inserting the partial-wave expansion of the fragmentation functions in Eqs. (25)–(26), we can rewrite the asymmetry in Eq. (10), for a proton target, as

$$A_{UT,p}^{\sin(\phi_R+\phi_S)\sin\theta}(x,y,z,M_{\pi\pi},Q) = -\frac{B(y)}{A(y)}\,\frac{|\boldsymbol{R}|}{M_{\pi\pi}}\,\frac{\sum_q e_q^2\, h_1^q(x)\, H_{1,sp}^{\sphericalangle,q}(z,M_{\pi\pi})}{\sum_q e_q^2\, f_1^q(x)\, D_1^q(z,M_{\pi\pi})} \tag{37}$$

For the specific case of the $\pi^+\pi^-$ final state, we can introduce into the flavor sum the

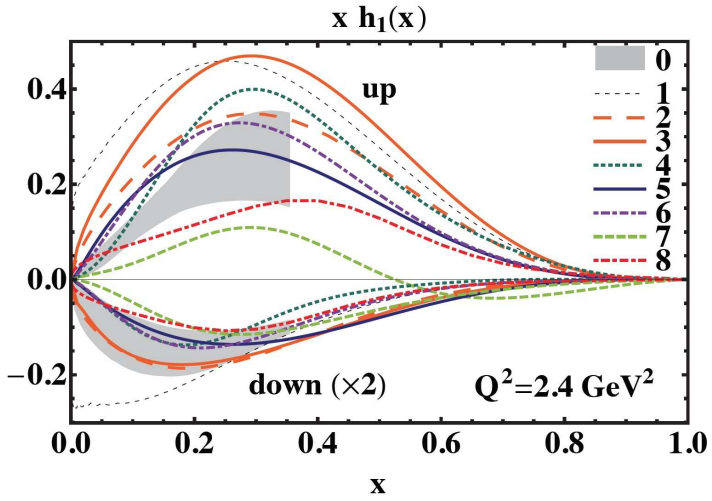


Figure 4: Model calculations of the transversity distribution function compared to available parametrization: (0–shaded band) extraction from ref. [58]; (1) saturated Soffer bound [59, 64]; (2) $h_1 = g_1$ [65]; (3-4) chiral quark-soliton models [66, 54]; (5) light-cone constituent quark model [67]; (6-7) quark-diquark models [53, 68], (8) quantum statistical approach [69].

constraints of Eqs. (27)–(31), and we get

$$A_{UT,p}^{\sin(\phi_R+\phi_S)\sin\theta}(x,y,z,M_{\pi\pi},Q) = -\frac{B(y)}{A(y)}\frac{|\boldsymbol{R}|}{M_{\pi\pi}}\frac{H_{1,sp}^{\sphericalangle,u}(z,M_{\pi\pi})\left[4h_1^{u-\bar{u}}(x)-h_1^{d-\bar{d}}(x)\right]}{D_1^u(z,M_{\pi\pi})\left[4f_1^{u+\bar{u}}(x)+f_1^{d+\bar{d}}(x)\right]+D_1^s(z,M_{\pi\pi})\,f_1^{s+\bar{s}}(x)} \quad , \tag{38}$$

where we adopt the compact notation $f_1^{q\pm\bar{q}}(x) = f_1^q(x) \pm f_1^{\bar{q}}(x)$, likewise for $h_1$. We neglected the contribution from charm quarks. For neutron targets, assuming isospin symmetry, we can simply interchange the role of $u$ and $d$ quarks in the PDFs.
Hence, for a deuteron target, we can rewrite the asymmetry for a $\pi^+\pi^-$ final state as

$$A_{UT,d}^{\sin(\phi_R+\phi_S)\sin\theta}(x,y,z,M_{\pi\pi},Q) = -\frac{B(y)}{A(y)}\frac{|\boldsymbol{R}|}{M_{\pi\pi}}\frac{H_{1,sp}^{\sphericalangle,u}(z,M_{\pi\pi})\,3\left[h_1^{u-\bar{u}}(x)+h_1^{d-\bar{d}}(x)\right]}{D_1^u(z,M_{\pi\pi})\,5\left[f_1^{u+\bar{u}}(x)+f_1^{d+\bar{d}}(x)\right]+D_1^s(z,M_{\pi\pi})\,2\,f_1^{s+\bar{s}}(x)} \quad . \tag{39}$$

We can use Eqs. (38)–(39) to extract the $u_v$ and the $d_v$ flavors separately. Defining

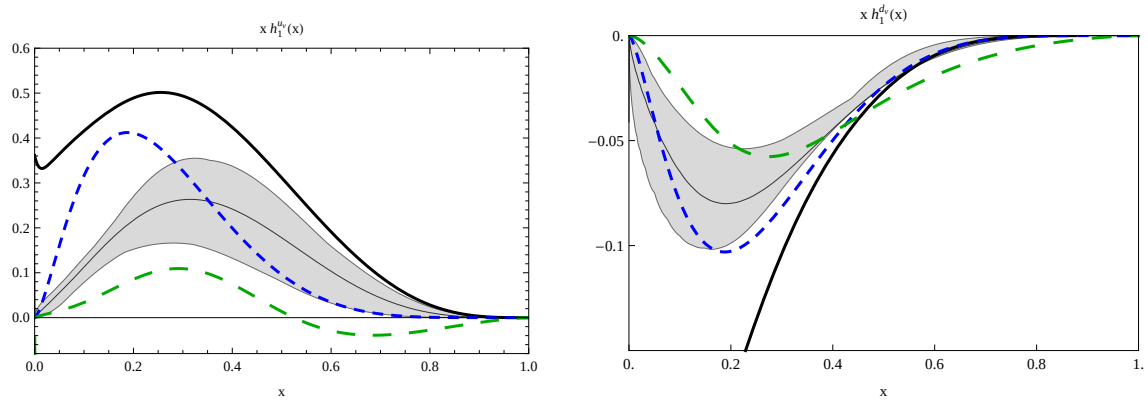


Figure 5: Estimates of $h_1(x)$ used in the present proposal for predictions, all evolved to 2.5 GeV$^2$. The blue short-dashed curve represents the LCCQM of Ref. [56], and the green long-dashed curve, the spectator model of Ref. [68]. The grey band is the extraction of Ref. [58]. The black curve is the Soffer bound evaluated with the LO MSTW08 unpolarized PDFs [70] and the LO DSS05 polarized PDFs [71].

$D_1^s = N_s D_1^u$ and turning to the notation of Eq. (33), with $0 \leq N_s \leq 1$, we find

$$
\begin{aligned}
h_1^{u_v}(x) &= \frac{1}{5}\,\frac{n_u}{n_u^\uparrow}\,\left(A_{UT,d}\,\left(\frac{5}{3}\left[f_1^{u+\bar{u}}(x) + f_1^{d+\bar{d}}(x)\right] + N_s\frac{2}{3}f_1^{s+\bar{s}}(x)\right)\right.\\
&\left. + A_{UT,p}\,\left[4f_1^{u+\bar{u}}(x) + f_1^{d+\bar{d}}(x) + N_s\, f_1^{s+\bar{s}}(x)\right]\right) \quad ,\\
h_1^{d_v}(x) &= \frac{1}{5}\,\frac{n_u}{n_u^\uparrow}\,\left(4A_{UT,d}\,\left(\frac{5}{3}\left[f_1^{u+\bar{u}}(x) + f_1^{d+\bar{d}}(x)\right] + N_s\frac{2}{3}f_1^{s+\bar{s}}(x)\right)\right.\\
&\left. - A_{UT,p}\,\left[4f_1^{u+\bar{u}}(x) + f_1^{d+\bar{d}}(x) + N_s\, f_1^{s+\bar{s}}(x)\right]\right) \quad . \qquad (40)
\end{aligned}
$$

We can now make the predictions for the asymmetries. The theoretical predictions do include the kinematical factors such as the depolarization factor. The binning chosen for the predictions on a proton target is given in Table 1. The coverage in $x$, which is much wider than for the previous experiments, is the strong point of this proposal.

In the collinear framework, which is of interest here, the dependence on the momentum fraction $x$ can be factorized from the $(z, M_{\pi\pi})$ dependence, but $z$ and $M_{\pi\pi}$ in general do not factorize. Their behavior has been studied in Refs. [44, 41]. Consequently, the dependence on ($z$, $M_{\pi\pi}$) is essentially determined by the DiFFs, while the dependence on $x$ comes only from the PDF.

In Figs. 6 and 7, we show the predictions for $A_{UT,p/d}^{\sin(\phi_R+\phi_S)\sin\theta}$ from Eqs. (38)–(39), respectively, at $Q^2 = 2.5$ GeV$^2$. When plotting the asymmetry as a function of $z$, it is understood that the other two variables have been integrated over in the observable range, and similarly for the other two combinations. In particular, the explored ranges are $0.075 \leq x \leq 0.532$, $0.3 \leq z \leq 0.8$, and $0.5 \leq M_{\pi\pi} \leq 0.9$ GeV.

| $M_{\pi\pi}$ bin |
|---|
| 0.5164 |
| 0.5655 |
| 0.6395 |
| 0.7157 |
| 0.7818 |
| 0.9066 |

| $z$ bin |
|---|
| 0.2949 |
| 0.4000 |
| 0.4649 |
| 0.5225 |
| 0.5775 |
| 0.6300 |
| 0.6825 |
| 0.7375 |
| 0.8000 |

| $x$ bin | $\langle Q^2 \rangle$ (GeV$^2$) |
|---|---|
| 0.0750 | 1.3 |
| 0.1120 | 1.4 |
| 0.1360 | 1.7 |
| 0.1599 | 1.9 |
| 0.1860 | 2.1 |
| 0.2160 | 2.3 |
| 0.2500 | 2.5 |
| 0.2880 | 2.8 |
| 0.3419 | 3.3 |
| 0.4000 | 4.1 |
| 0.4600 | 5. |
| 0.5320 | 6.3 |

Table 1: Binning in $z, M_{\pi\pi}$ and $x$ used in Fig. 6 for the predictions for the SSA asymmetry on proton target (HD-Ice) as well as the average value for $Q^2$ for the corresponding $x$-bin. The binning is slightly different for the deuteron target.

The red points correspond to results obtained when using the $x$-dependence of the Torino parametrization for the transversity [58]. The blue points are produced when using the PDFs from the Light-Cone Constituent Quark Model (LCCQM) of Ref. [67], evolved at LO to 2.5 GeV$^2$. Since this model assumes $SU(6)$ symmetry for the proton state, in this case the asymmetry in Eq. (38) becomes

$$A_{UT}^{\sin(\phi_R+\phi_S)\sin\theta}(x,y,z,M_{\pi\pi},Q) = -\frac{B(y)}{A(y)}\,\frac{|\boldsymbol{R}|}{M_{\pi\pi}}\,\frac{\left(4+\frac{1}{4}\right)\,h_1^u(x)\,H_{1,sp}^{\sphericalangle,u}(z,M_{\pi\pi})}{\left(4+\frac{1}{2}\right)\,f_1^u(x)\,D_1^u(z,M_{\pi\pi})} \quad . \tag{41}$$

The black points refer to the results from the spectator diquark model of Ref. [68], again evolved at LO to 2.5 GeV$^2$. In this model, there is no specific flavor symmetry [63] and the asymmetry becomes

$$A_{UT,p}^{\sin(\phi_R+\phi_S)\sin\theta}(x,y,z,M_{\pi\pi},Q) = -\frac{B(y)}{A(y)}\,\frac{|\boldsymbol{R}|}{M_{\pi\pi}}\,\frac{H_{1,sp}^{\sphericalangle,u}(z,M_{\pi\pi})\,\left(4h_1^u(x)-h_1^d(x)\right)}{D_1^u(z,M_{\pi\pi})\,\left(4f_1^u(x)+f_1^d(x)\right)} \quad . \tag{42}$$

The $\sin(\phi_R+\phi_S)\sin\theta$ asymmetry has already been studied at HERMES and COMPASS, in different kinematics and on different targets. This made it possible to extract the relevant combinations of the $u_v$ and $d_v$ transversity distributions, namely $xh_1^{u_v} - xh_1^{d_v}/4$ for a transversely polarized proton target, and $xh_1^{u_v} + xh_1^{d_v}$ for a trans-

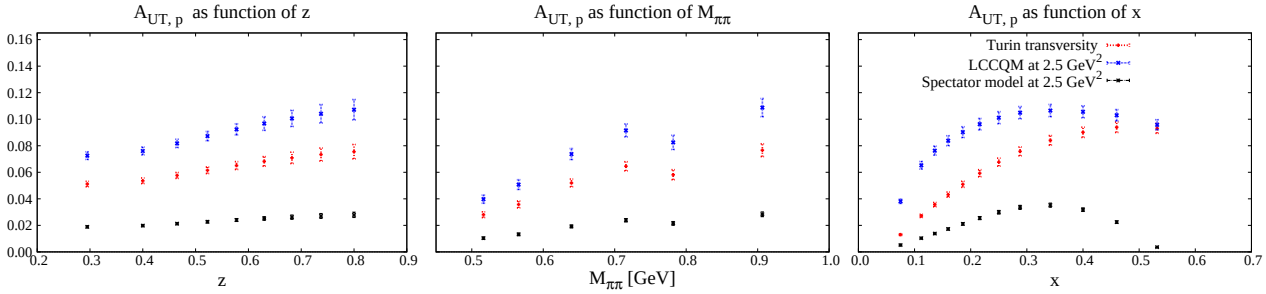


Figure 6: Predictions for the asymmetry $A_{UT,p}^{\sin(\phi_R+\phi_S)\sin\theta}$ in ($z$, $M_{\pi\pi}$, $x$) (Eq. (38)). The red points are deduced from the $x$-dependence of the transversity in Ref. [58] together with the MSTW08 unpolarized PDFs. The blue points are from the LCCQM in Ref. [56]; and the black points are from the spectator model of Ref. [72]. The average scale is $Q^2 = 2.5$ GeV$^2$.

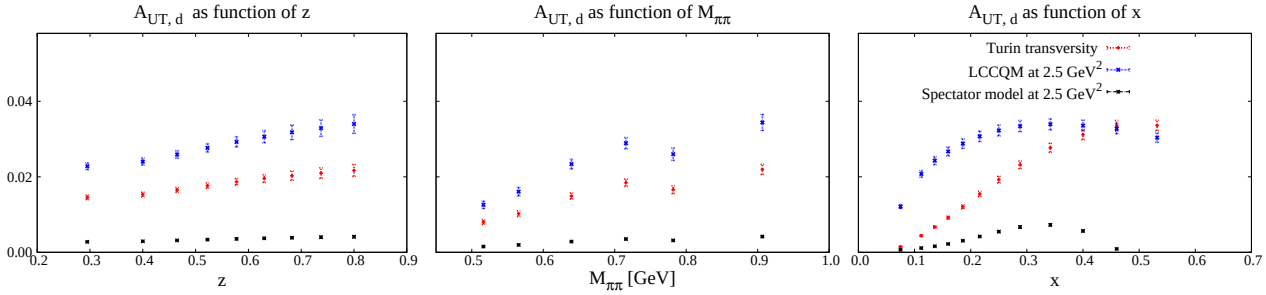


Figure 7: Same as Fig. 6 except for $A_{UT,d}^{\sin(\phi_R+\phi_S)\sin\theta}$ in ($z$, $M_{\pi\pi}$, $x$) (Eq. (39)).

versely polarized deuteron target. In fact, using Eqs. (38,39) we get

$$\left[x h_1^{u-\bar{u}}(x) - \frac{x}{4}\, h_1^{d-\bar{d}}(x)\right] = -\frac{A(y)}{B(y)}\, A_{UT,p}^{\sin(\phi_R+\phi_S)\sin\theta}\, \frac{n_u}{n_u^{\uparrow}} \left[x f_1^{u+\bar{u}}(x) + \frac{x}{4}\, f_1^{d+\bar{d}}(x) + \frac{N_s}{4}\, x f_1^{s+\bar{s}}(x)\right] \quad , \tag{43}$$

$$\left[x h_1^{u-\bar{u}}(x) + x h_1^{d-\bar{d}}(x)\right] = -\frac{A(y)}{B(y)}\, A_{UT,d}^{\sin(\phi_R+\phi_S)\sin\theta}\, \frac{n_u}{n_u^{\uparrow}} \left[\frac{5}{3}\left(x f_1^{u+\bar{u}}(x) + x f_1^{d+\bar{d}}(x)\right) + \frac{2N_s}{3}\, x f_1^{s+\bar{s}}(x)\right] \quad . \tag{44}$$

In Fig. 8, we show the results from Eq. (43) for the proton target [73, 74]. In Fig. 9, we refer to Eq. (44) in Ref. [74]. In both cases, the effects of QCD evolution have been properly taken into account at LO in $n_u/n_u^{\uparrow}$ and in the unpolarized PDFs, including the dependence $Q^2(x)$ of the hard scale on each different experimental $x$ bin.

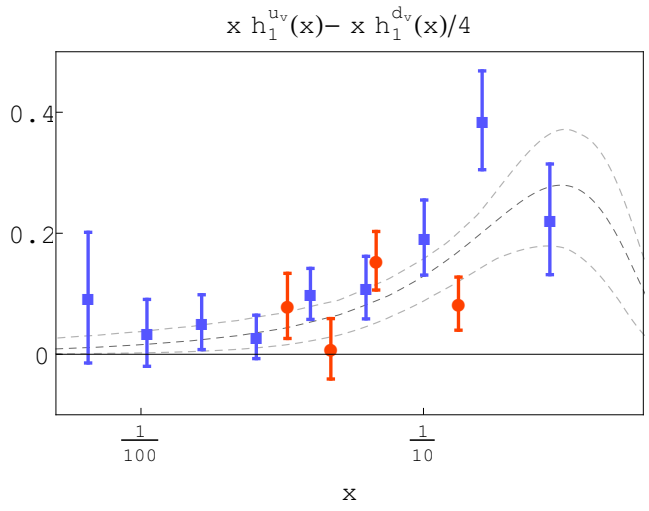


Figure 8: Transversity for the combination $h_1^{u_v} - 1/4 h_1^{d_v}$ extracted via DiFFs [73, 74], using the COMPASS data for proton (2007) (blue dots) and HERMES data for proton (red dots). The grey curves correspond to the Torino extraction with error bands (calculated with $\Delta\chi^2 = 15$).

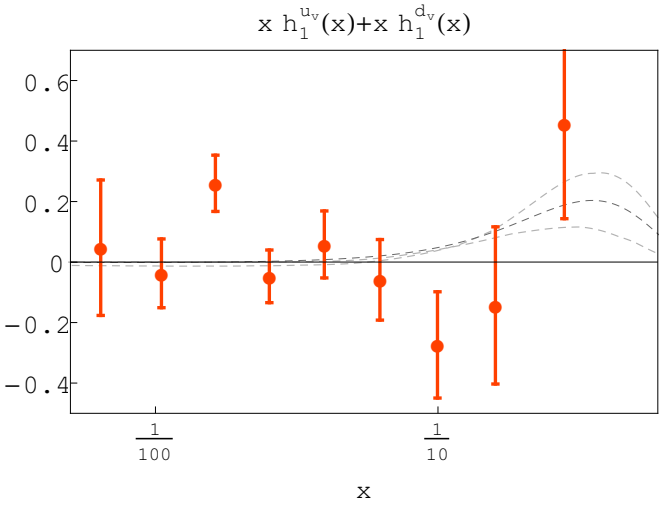


Figure 9: Transversity for the combination $h_1^{u_v} + h_1^{d_v}$ extracted via DiFFs [74], using the COMPASS data for deuteron (2002-2004) (red dots). The grey curves correspond to the Torino extraction with error bands (calculated with $\Delta\chi^2 = 15$).

# 4 The Present Experiments and JLab Proposals

Target spin asymmetries in dihadron production have been published by the HERMES Collaboration on the proton [27] and the COMPASS collaboration on deuterium and proton targets [28]. Kinematics at HERMES and in particular at COMPASS is limited to relatively low $x$, where the transversity PDF is not expected to be large (see Fig 8). The physics of hadron pair production at JLab has been discussed only for unpolarized and longitudinally polarized targets [75], where the target asymmetries are higher twist.

The large acceptance of CLAS12 will allow measurements of pions pairs in SIDIS over a wide range in $x, Q^2$. Important advantages of the proposed configuration using HD-Ice target are the large acceptance (no strong holding field is required) and the negligible nuclear background. In particular wide $Q^2$, provides control over possible higher twist contributions. With respect to nuclear targets ($NH_3$, $ND_3$), the HD-Ice dilution factor is a factor of 2 better at small $P_{h\perp}$ of hadrons, and goes up to a factor of 6 at $P_{h\perp} > 0.8$ GeV [76]. A good dilution factor at large $P_{h\perp}$ is crucial for control over the systematics due to integration over the hadronic transverse momenta. Wide acceptance of the CLAS12 spectrometer and the capability to measure multi-particle final states will allow the simultaneous measurements of asymmetries as a function of the missing mass of the hadron pair, allowing separation of exclusive contributions. Projected statistical errors for this proposal are shown in Section 5.3.

# 5 A Dedicated SIDIS Experiment with a Transversely Polarized Target and CLAS12

The main goal of the proposed experiment is to measure the $x$, $z$ and $M_{\pi\pi}$ dependences of the target single-spin asymmetries in the accessible kinematics in $x$, $Q^2$ (Fig. 10). The target single spin asymmetry, $A_{UT}$, will be calculated in bins of $\phi_R + \phi_S$ and $\theta$ as:

$$A_{UT}(\phi_R, \theta) \;=\; \frac{1}{f P_t} \frac{(N^+ \;-\; N^-)}{(N^+ \;+\; N^-)} \;, \tag{45}$$

where $P_t$ is the target polarization (with respect to the electron beam direction), $f$ is the dilution factor, i.e. the fraction of events from the polarized material of interest (H or D), and $N^{+(-)}$ are the charge-normalized extracted number of $ep^\uparrow \;\rightarrow\; e\pi^+\pi^- X$ events for opposite orientations of the transverse spin of the target.

The proposed experiment will provide statistically significant measurements of the kinematic dependences of the target SSA in dihadron production.

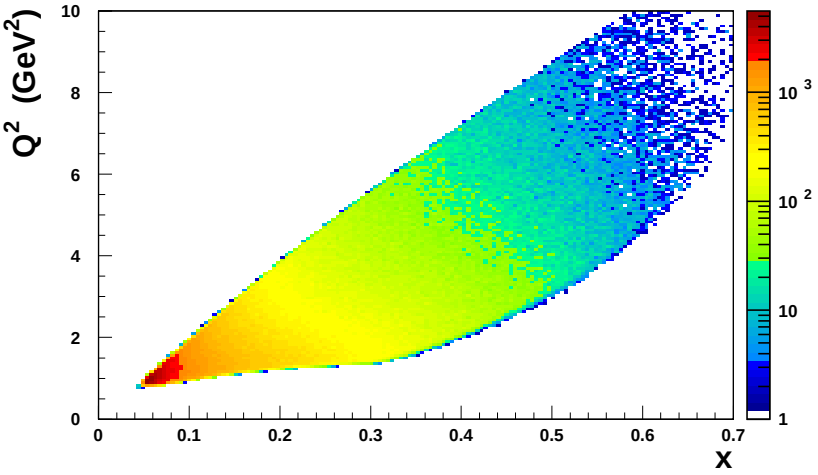


Figure 10: Kinematic coverage of CLAS12 with the transverse target.

## 5.1 The CLAS12 Configuration

The proposed experiment will use the upgraded CLAS12 spectrometer in its standard configuration, together with the transversely polarized HD-Ice target, which will include an additional compensation magnet to shield the target region so the transverse target magnet can operate.

### 5.1.1 The HD-Ice Transversely Polarized Target

A transversely polarized target in a frozen-spin state, such as the HD-Ice target, requires only relatively small holding fields, which greatly mitigates background problems associated with beam deflection due to the large magnetic fields. This potentially allows to avoid installation of the magnetic chicane to bend the electron beam, deflected by the strong holding field of traditional targets, also generating additional bremsstrahlung. In addition, the HD-Ice target has limited dilution. The only non polarizable nucleons are associated with the target cell and these can be sampled and subtracted in conventional empty-cell measurements. At the same time, the low Z results in a long radiation length and comparatively few bremsstrahlung photons.

The factors affecting target polarization are complex and intertwined. At BNL, HD target polarizations of 60% H and 35% D were achieved in photon experiments with spin relaxation times in excess of a year. Hydrogen relaxation times require fields $\int BdL = 0.050$ T-m, which is about 30 times less than a dynamically polarized

ammonia target.

The HD-Ice target has been developed for tagged photon beam operation and is now in use with the CLAS detector employing a new In-Beam-Cryostat (IBC) and the tagged photon facility in Hall B. The target has been used successfully to measure beam-target double polarization asymmetries on protons and on neutrons (deuterium). A tagged photon rate of $10^8$ per second has been used over many weeks of operation without measurable polarization decays due to beam heating or radiation damage. While the operation in photon beam showed very promising performance of the HD-Ice target, the use of the HD target material in electron beams requires modifications to the heat extraction from the HD material, which was designed for the low beam power when operating the target in photon beams. This requirement affects two technical design aspects of the target for use with intense electron beams, (1) the cooling power of the CLAS IBC and (2) the heat extraction and transport from the HD material to a heat sink. It may also affect (3) the decay time constants of the HD material due to possible more severe radiation damage. An electron beam test was conducted in March in Hall B to obtain empirical information about modifications to the IBC to deal with (1) and (3). The results are briefly summarized here:

- In preparation for the electron beam test, the cooling power of the IBC was increased 3-fold using additional roots pumps. This allowed to keep the cryostat temperature below 160mK using electron currents of 1nA rastered over the 1.5cm diameter target front face. This will be adequate to operate the IBC at luminosities of up to L=$4.10^{33}$ $cm^{-2}s^{-1}$. However, an additional factor of 3 improvement in cooling power is achievable with the existing IBC and pumping units.

- Heat extraction from the HD material is currently achieved with hundreds of thin aluminum wires of high purity. This design was optimized for photon running and is known to be insufficient for heat extraction with the much higher energy deposition during electron operation. A different design and some R&D work will be needed to develop a new target cell with much improved heat extraction. This could not be done in time when the electron test was conducted. The beam test was therefore limited to low current operation (0.25-1.0 nA). Even at operation of 1nA or less local heating of the HD cell was present that caused polarization decays during beam operation.

- The most important result from the test is due to possible radiation damage. This was tested by exposing the target to 1nA beam current over a 12 hours period. After this beam exposure, the beam was turned off and the relevant time constant T1 was determined. Due to the very long time constant and uncertainties in the NMR measurement only a lower limit of T1 $>$ 50 days could be established.

To avoid radiation damage to the target the beam will be rastered over the target

surface in a spiral pattern. The beam position is measured indirectly by recording the simultaneous currents of the raster magnet. These values can be used off-line to correct for effects of the raster on the vertex z-position. The raster magnets may be also used to give a small angle ($\sim 0.1^{o}$) to the incident electron beam, so that beam at target center will be collinear with the z-axis to confine bremsstrahlung photons into the beam pipe.

The main result of the electron beam test strongly indicates that radiation damage is not causing a rapid decay of the hydrogen polarization at luminosities that are anticipated for this proposal. A remaining technical problem is the heat extraction from the HD material that may require specific R&D work and a refined beam rastering system for use in intense electron beams. As a consequence the present proposal assumes a target not longer than the present one.

The composition for a 5 cm solid HD target with 2.5 cm diameter is shown in the Table 2. Frozen-spin HD, thus, provides a very attractive alternative for electron experiments in particular with transversely polarized targets.

Table 2: HD-Ice target materials

| Material | gm/cm$^2$ | mass fraction (%) |
|---|---|---|
| HD | 0.735 | 78% |
| Al | 0.139 | 15% |
| $C_2ClF_3$ | 0.065 | 7% |

The baseline of CLAS12 detector is based on two superconducting magnets. The large 2 T toroid magnet is used by the forward spectrometer as particle momentum analyzer. The 5 T main solenoid of the central detector allows particle momentum determination in the backward region and constrains the large Møller background within the beam pipe.

The insertion of a transverse target in CLAS12 requires a volume where the longitudinal field of the main solenoid is shielded. In the shielded region a transverse target magnet can operate. A solution for a 3 T field and 10 cm long target was proposed at PAC38 to work at $10^{34}$ cm$^{-2}$s$^{-1}$ luminosity.

The recent HD-Ice test with electron beam indicates that the relaxation time of the polarization is not significantly altered by the beam exposure but the heat extraction from the HD material has to be improved. To account for this, a target not-longer than the present one (5 cm) and thus a luminosity of $5 \cdot 10^{33}$ cm$^{-2}$s$^{-1}$, more than an order of magnitude lower than the one affordable with the CLAS12 detector, is here assumed.

In this condition the requirements for the magnetic configuration to shield the longitudinal field of the main solenoid in the target region are less stringent. The Møller background reduces proportionally to the luminosity and can be contained with a limited solenoidal field: ongoing MC studies show that a 2 T field would

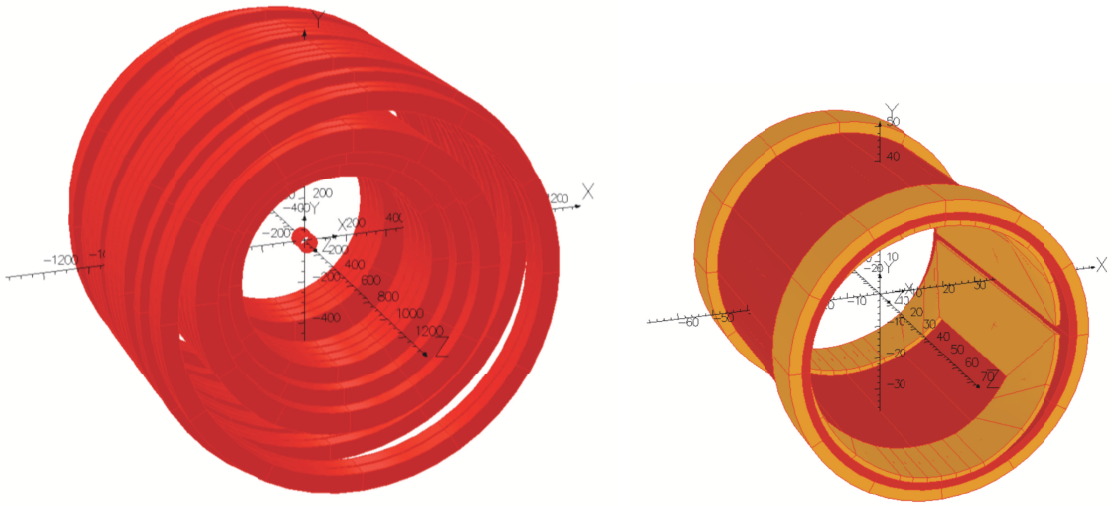

Figure 11: (Left) The HD-Ice superconducting magnetic system surrounds the target at the center of the CLAS12 central detector solenoid. (right) The HD-Ice magnetic system comprises, moving outward from the beam line, the HD-Ice holding field saddle coil (brown), the compensating solenoid (red), and the Helmholtz coil (brown).

be enough, see Sec. 5.1.3. The shorter target allows a better compromise between acceptance and holding field uniformity.

In the present design the longitudinal field compensation and the transverse field are generated by superconducting coils internal to the HD-Ice liquid helium can, with almost no impact on the CLAS12 detector configuration. The proposed HD-ice magnet design is basically an enhanced version of the present coil system already in use with the current HD-Ice.

The HD-Ice target requires a highly (better than $10^{-3}$) uniform field for polarization measurement by NMR technique. This is accomplished by the central detector solenoid, able to provide a field uniformity better than $10^{-4}$ in the limited target volume. As a consequence, the present long NMR solenoid coil inside the liquid helium can of the HD-Ice cryostat can be shortened to become part of the longitudinal field compensating system, designed to provide a open forward acceptance greater then 35 degrees. The system is completed by an Helmholtz pair of coils, which improves field uniformity and concentrates the material budget in the not-crucial 35-50 degrees transient between current region (forward detector for SIDIS kinematics) and recoil region (central detector for DVCS recoiling proton). The adopted superconducting magnetic configuration, optimizing the acceptance, field uniformity and the material budgetis shown on Fig. 11.

The compensating system is designed to not interfere with the CLAS12 forward acceptance up to angles greater than 35 degrees. It allows the detection of DVCS recoil

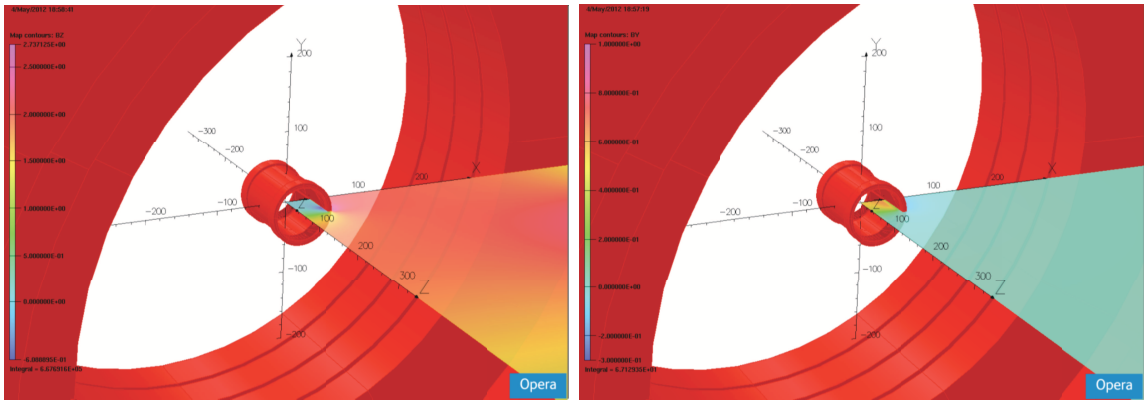


Figure 12: (Left) the 2 T longitudinal field component is almost compensated to zero internal to the HD-Ice magnetic system. (Right) The 0.5 T transverse target holding field is limited to a small volume around the HD-Ice target.

protons, although with a limited resolution due to the additional material budget associated with the superconducting coil intercepting the recoil proton acceptance. A saddle coil has been added to the system to provide up to 0.5 T transverse field holding the target polarization. The main parameters of the correction magnets are listed in Table 3. The resulting main field components are depicted in Fig. 12.

Table 3: Main parameters of the magnet assembling.

| parameter | Central detector solenoid (ideal) | Saddle coil | Compensat. solenoid | Compensat. Helmholtz |
|---|---|---|---|---|
| inner radius (mm) | 471 | 35.8 | 37.4 | 38.4 |
| outer radius (mm) | 650 | 37.4 | 38.4 | 41.8 |
| length (mm) | 1225 | 100 | 100 | 15 |
| current density (A/mm$^2$) | | 730 | 730 | 730 |

An important parameter is the uniformity of the transverse field holding the target polarization. The surviving longitudinal component of the field in the target volume is not higher than 5 mT for a target length up to 5 cm. Experimentally the target transverse polarization is defined with respect to the beam, whereas the component relevant to theory is the one transverse to the virtual photon. The angle between the beam and the virtual photon is approximately given by $\sin\theta_{e\gamma^*} \approx \gamma\sqrt{1-y}$ with $\gamma = 2xM/Q$ and M the proton mass. As a consequence, the target spin actually has a longitudinal component (with respect the virtual photon), which can be as high as $\pm$ 15%. The influence on transverse analyses has been studied in detail at HERMES [8, 77], and quantified as negligible. This fixes the order of magnitude

of the tolerable longitudinal field component into the target volume, which is much higher than the one obtained with the present configuration and a transverse field of 0.5 T.

The static forces acting on the coils of the HD-Ice magnetic system were evaluated to be smaller than 10 MPa, a value well below the 300 MPa tensile strength of the G10 epoxy usually used in superconducting coils assembling. Small misalignments, of the order of 1 mm, of the HD-Ice target system with respect the magnetic center of the central detector solenoid do not generate significant forces as the target sits in a region of pretty uniform field.

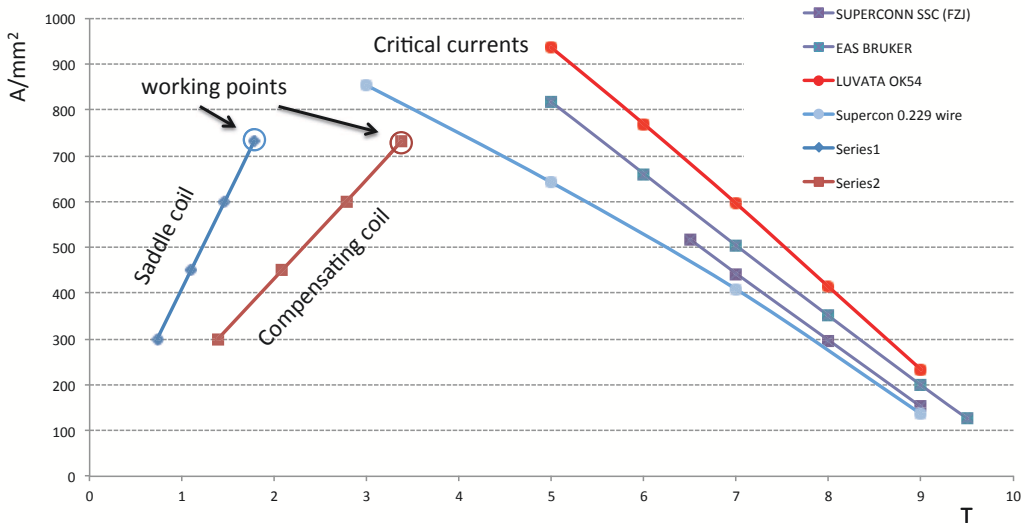


Figure 13: Load lines of the compensating (dark red) and saddle (dark blue) coils as compare to the critical current of the considered superconducting wires (see text). A realistic filling factor of 80% is considered for the superconducting coil wiring. The arrow indicates the working points.

The load line of the compensating solenoid are shown in Fig. 13, where different superconducting NbTi wire performances are reported: the SUPERCON 0.229 wire used in the CLAS HD-Ice target, the SUPERCON wire used by the PAX experiment at FZJ (VSF/SSCI), together with the F54 wire by BRUKER/EAS and the OK54 wire by LUVATA/OUTOKUMPU. The working point at 730 A/mm$^2$, corresponding to the proposed configuration, is below the critical current of commercially available superconducting wires, in particular the one used for the present HD-Ice run at CLAS. As a quench can not be excluded due to external accident, the coils were dimensionated in order to allow the use of a standard quench protection. From the magnetic point of view, the safety margin gives freedom in future geometry optimization for i.e.

a reduction of the material budget or a better compromise between field uniformity and acceptance.

In conclusion, a magnetic system internal to the liquid helium can of the HD-Ice target can be used to compensate the central detector longitudinal field in the target volume. The coils can be wound with existing standard commercial wires and work with an acceptable safety margin. Work is in progress to optimize the performances of the system.

### 5.1.2 Target Polarization Measurements

The target polarization will be measured with an NMR system [78, 79, 80]. Polarimetry for nuclear targets has been studied extensively at BNL. The In-Beam-Cryostat that will hold HD targets within CLAS12 will have a short saddle coil to maintain transverse spin orientations. Keeping this coil short will both reduce the $BdL$ deflection of electrons, as well as minimize spin diffusion from radiation damage (by changing the Larmor frequency across the target). However, the fields associated with this coil will be too non-uniform for NMR measurements. Instead, the central detector solenoid, able to provide a $10^{-4}$ field uniformity within the target volume, will be used for NMR polarization monitoring. The target spins will readily follow the field as the HD-Ice magnetic system (compensating and saddle coils) is ramped down. NMR data will be collected after which the HD-Ice magnetic system will be ramped up. We anticipate a total cycle time of about 30 minutes (limited by how fast the fields can be changed without quenching the magnets), enabling NMR data to be collected a couple of times per day. The systematic uncertainties in HD polarization are about 4% (relative). The largest single factor (contributing 2.8% relative) is the differential uncertainty on the gain of a lock-in amplifier whose scale must be changed by many orders of magnitude between equilibrium-polarization measurements and high-polarization frozen-spin measurements. Separation of signal and background in the calibration measurements contributes at the 1% level.

An additional estimate of the product of target and beam polarizations, $P_B P_t$, will be done also off-line by comparing the well known $ep$ elastic asymmetry

$$A_{theo} = -\frac{\cos\theta_\gamma\sqrt{1-\epsilon^2} + (\frac{Q^2}{4M^2})^{-\frac{1}{2}}\sqrt{2\epsilon(1-\epsilon)}\sin\theta_\gamma\cos\phi_\gamma\frac{G_E}{G_M}}{\epsilon(\frac{Q^2}{4M^2})^{-1}(\frac{G_E}{G_M})^2 + 1} \tag{46}$$

with the measured asymmetry

$$A_{meas} = \frac{N^+ - N^-}{N^+ + N^-} = \frac{P_B P_t \sigma_{et}}{\sigma_0} \equiv P_B P_t A_{theo}. \tag{47}$$

For the ratio $\frac{G_E}{G_M}$, we will use values from polarization transfer measurements [81], which are expected theoretically to have the same (small) two-photon corrections as $A_{LT}$ measurements. On average, the uncertainty in $A_{LT}$ due to $G_E/G_M$ will be

about 2% (relative). The measurements will consist of measuring both an electron and a proton, and imposing missing momentum and energy cuts to isolate the elastic channel. Events from H and D will be distinguished through a multi-parameter fit to the missing mass and energy distributions. Fermi broadening in the deuteron generates peaks that are typically twice as wide as for hydrogen, for the conditions of this proposal. Due to this mixing, the errors will be approximately 1.4 times bigger than for targets which contain only H or D plus heavy materials such as nitrogen or aluminum.

The beam polarization will be measured periodically with the standard Hall-B Møller polarimeter.

### 5.1.3 The Impact of Møller Scattering

One of the main sources of background produced by a high-energy electron beam impinging upon a HD target is due to interactions of the electron beam with the atomic electrons (Møller scattering). This rate is several orders of magnitude larger than the inelastic hadronic production rate. A dedicated Monte Carlo study aimed at evaluating the impact of the Møller scattering on the detector occupancies has been performed using the CLAS12 GEANT4 based MC (gemc). The effect of HDice magnetic configuration on Møller electrons is depicted in Fig. 14, indicating an efficient screen of the background is feasible also with the transverse target magnet configuration.

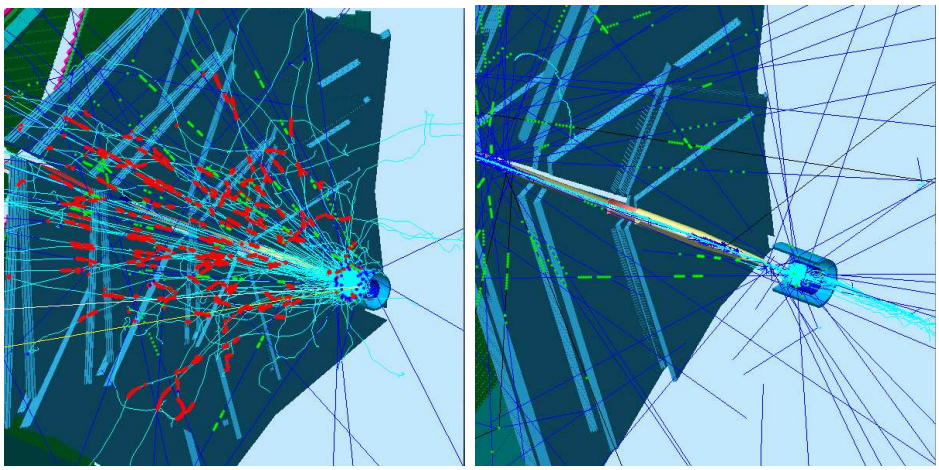

Figure 14: Comparison of the CLAS12 response without (left) and with (right) the magnetic field of the HDice magnet configuration. The blue lines are photons, the cyan are electrons. Green points only indicate the passage of the photons through DC with no energy deposition.

The HD-Ice in-beam cryostat will be modified to optimize the target magnet

configuration and achieve maximum uniformity for acceptable occupancies in the CLAS12 DC. The CLAS12 response to a single SIDIS event in gemc is shown in Fig. 15. The CLAS12 DC occupancies with the HD-Ice magnet configuration and a luminosity of $5 \cdot 10^{33}$ cm$^{-2}$s$^{-1}$, are below 2%, see Fig. 15. This is comparable (slightly worse) with the less than 1% occupancy achieved in the nominal CLAS12 configuration, corresponding to 5 T longitudinal field and $10^{35}$ cm$^{-2}$s$^{-1}$.

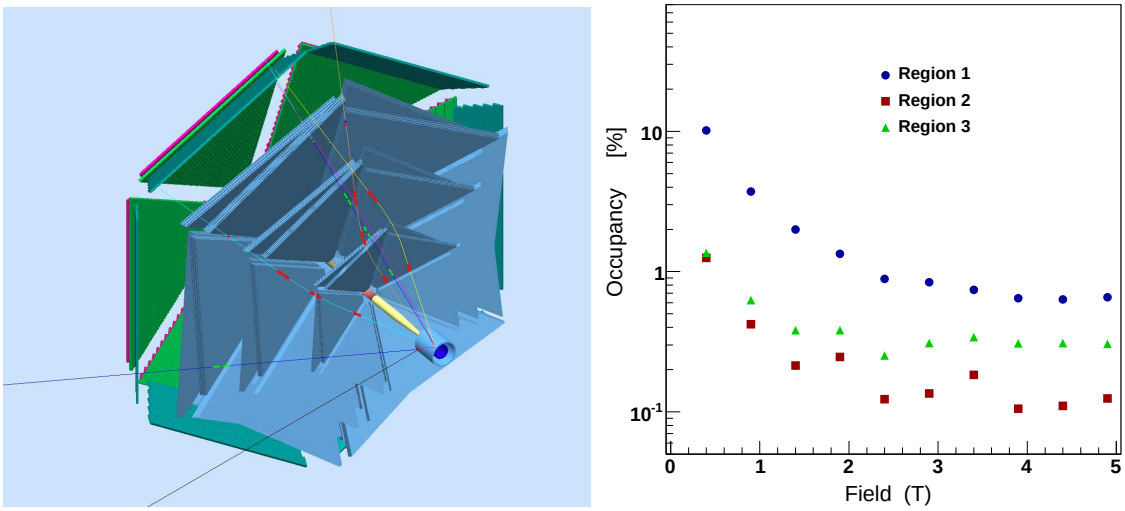


Figure 15: (Left) A SIDIS event in CLAS12 from gemc simulation. (Right) CLAS12 DC occupancies with the HD-Ice transverse magnetic system at $5 \cdot 10^{33}$cm$^{-2}$s$^{-1}$, as a function of the central solenoid field strength. The foreseen working point is at 2 T.

## 5.2 The Measurement

### 5.2.1 Event Reconstruction

Final-state hadrons and the scattered electron will be detected by the CLAS12 spectrometer. The HD-Ice and its magnet configuration have been implemented in the GEANT4 simulation of the CLAS12 to study the reconstruction efficiencies and resolutions in the presence of the transverse field of the HD-Ice target.

The corresponding resolutions for charged particles, which are the main concern, are shown in Figs. 16, 17. The resolution on the forward electron track meets the specification of the CLAS12 technical design report, except for the angle measurement at low momentum. The reconstruction of the large-angle proton track is worse but not far from the resolutions in momentum and polar angle achievable with nominal CLAS12 configuration, which are 6% and 7 mrad, respectively. The proton angular resolution is limited by the straggling in the HD-ice magnet coils expecially at low

momenta, whereas its momentum resolution is limited at large momenta by the reduced field of the central detector solenoid. These preliminary study was performed with a oversimplified description of the HD-Ice magnetic system and in-beam cryostat, resulting in a substantial overestimation of the material budget effect. A more realistic geometry is under study.

### 5.2.2 Event Identification

Electrons are separated from heavier particles using Cherenkov counters and electromagnetic calorimeters. Pions will be identified using Cherenkov counters and measurement of time of flight. Pion momenta will be reconstructed in the CLAS12 drift chamber system, embedded within the toroidal magnetic field. Kinematic distributions of electrons and final state hadrons are shown in Fig. 18.

Electron detection at large angles (larger than 20 degrees) is important to explore the large $Q^2$ regime. The CLAS12 forward detector is perfectly suitable for such measurements since designed to cover up to 40 degrees angles, relevant for measurements of hadron pairs.

### 5.2.3 Acceptance and Data Analysis

Although SSAs are typically not too sensitive to acceptance corrections, in the case of the transverse target, due to the large number of contributions appearing as different azimuthal moments in the cross section, the acceptance corrections are more important. The analysis of the transverse target requires fits in the 2-dimensional space of the relevant azimuthal angles $\phi_R$ and $\phi_S$. A detailed procedure on the accounting for acceptance corrections in the separation of the different azimuthal moments was developed by the HERMES collaboration. According to this method, a fully-differential (thus free from acceptance effects) parametrization of the asymmetries is extracted from the data itself with a fully-unbinned maximum likelihood fit. The parametrization is then used in input to a Monte Carlo simulation which accounts for a complete model of the instrumental effects (acceptance, smearing, inefficiencies...) to generate a pseudo-data sample. The systematic effects are evaluated as the difference of the asymmetries extracted from the pseudo-data sample and the parametrization in input to the Monte Carlo. A similar procedure has been applied to estimate the expected acceptance corrections for e.g. the Collins asymmetry as extracted in the CLAS12 acceptance.

### 5.2.4 Count Rates and Statistical Errors

With the proposed configuration as described in Section 5.1, a luminosity of $5.10^{33}$ $\mathrm{cm}^{-2}\mathrm{s}^{-1}$ is expected. The yields of SIDIS hadrons are estimated using a Monte Carlo simulation of the acceptance and smearing of the detector, based on the PYTHIA generator tuned to the multiplicities measured at the HERMES experiment. The

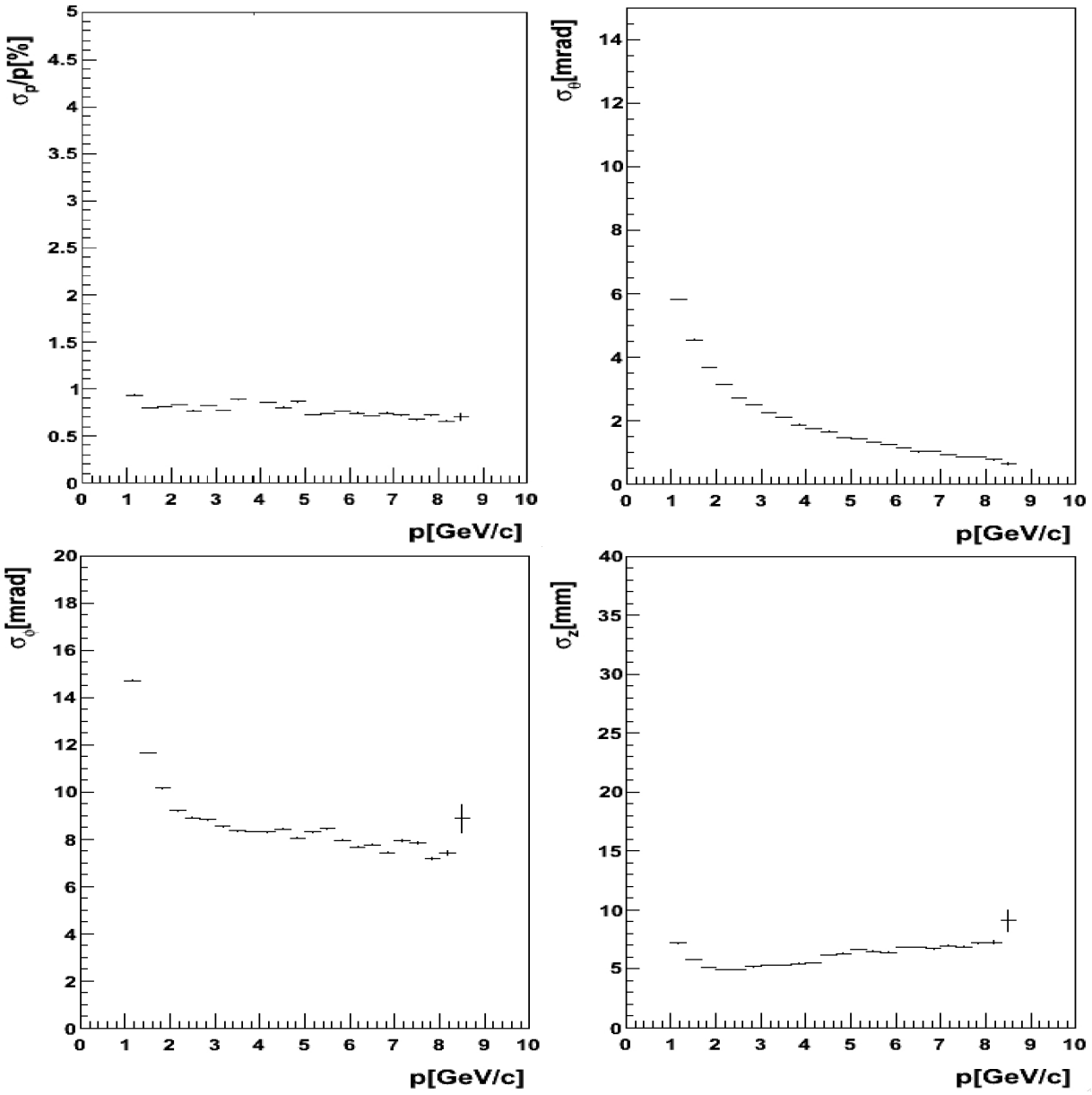


Figure 16: Resolutions in momentum, polar angle, azimuthal angle and reconstructed vertex for forward charged tracks (electrons) from CLAS12 reconstruction program. Reconstruction of events was performed using the input from the GEANT4 simulation, accounting for the HD-Ice configuration and transverse field of the target.

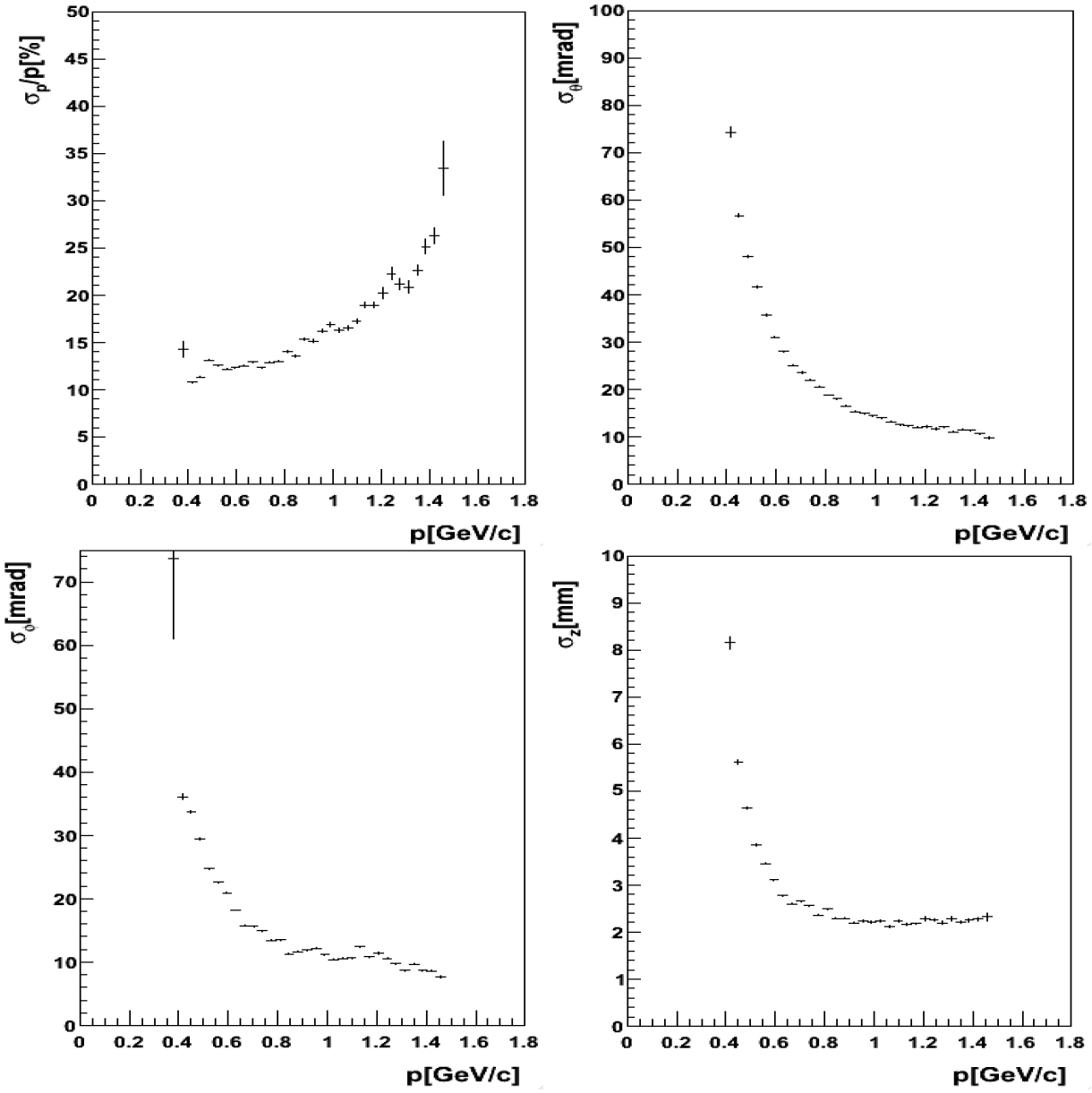


Figure 17: Resolutions in momentum, polar angle, azimuthal angle and reconstructed vertex for large angle charged tracks (protons) from CLAS12 reconstruction program. Reconstruction of events was performed using the input from the GEANT4 simulation, accounting for the HD-Ice configuration and transverse field of the target.

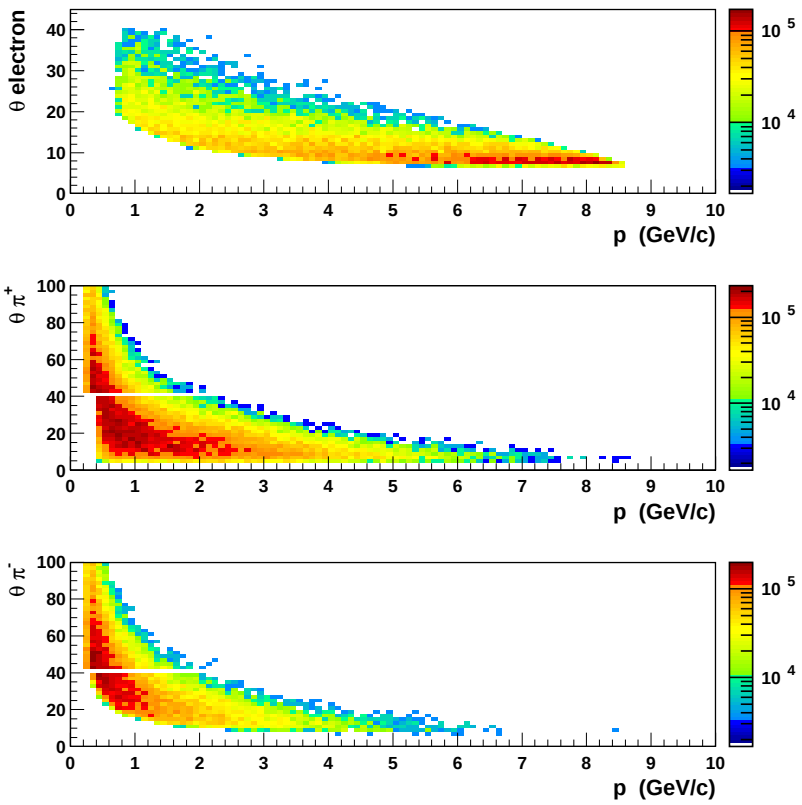


Figure 18: Kinematic distributions of electrons and final state hadrons.

statistics of the proposed experiment is calculated for 100 days of data-taking (i.e. for the total requested beam time, 110 days, diminished by a 10% duty-factor accounting for calibration runs, empty target runs, and supportive tests). The expected number of SIDIS pion pairs within the kinematic limits: $Q^2 > 1$ GeV$^2$ (corresponding to $x > 0.05$), $W^2 > 4$ GeV$^2$, $0.10 < y < 0.85$ and $0.3 < z < 0.8$ are $\sim 8$ M for $\pi^+/\pi^-$ pairs. A squared missing mass greater than 2 GeV$^2$ was required to suppress the contamination form exclusive channels.

In calculations of the statistical uncertainties on the asymmetries (see Section 5.3) the hydrogen target polarization is assumed to be 60% and a dilution factor for the hydrogen target of the order of 1/3.

The number of days was chosen to achieve a statistical error that is not significantly larger than the systematical error at the highest $x$.

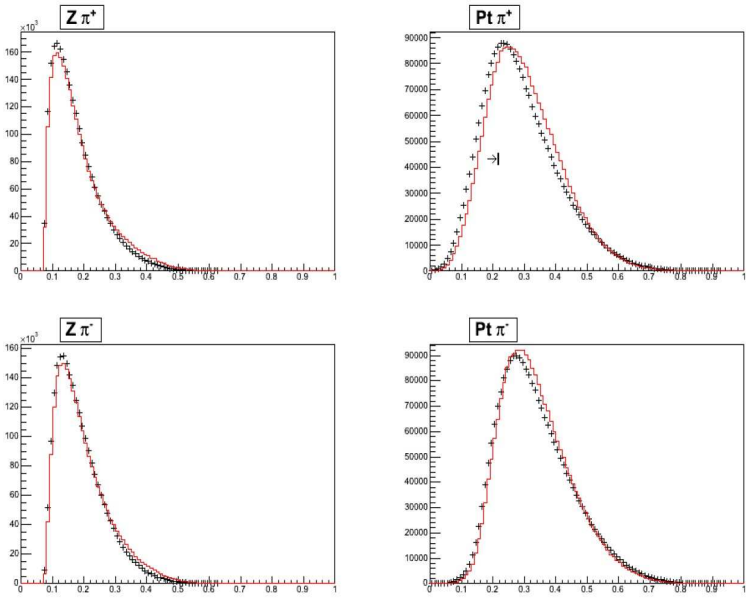


Figure 19: Comparison of transverse momentum and $z$ of charged pions with simulation (PEPSI+GEANT simulation of the CLAS eg1dvcs setup) of dihadrons at 6 GeV with CLAS eg1dvcs data on pion pair electroproduction at 6 GeV.

### 5.2.5 Systematic Errors

The systematic uncertainties can be divided into two categories: those that scale with the measured asymmetry and those that are independent of the measured results. In the first category, the dominant uncertainty is expected to be that from the target polarization and the dilution from the target material other than HD (see table 2). For the second category, we have taken our best estimate of the magnitude of the systematic effect, and divided by the average expected proton asymmetry.

One of the main contributions to the estimated relative uncertainties, summarized in Table 4, comes from the procedure used to separate the azimuthal moments of interest one from other and potentially non-zero, azimuthal asymmetries (for example a twist-3 $\sin(\phi_S)$ moment). Systematics due to acceptance effects have been studied using the PEPSI (based on the PYTHIA) generator and the FASTMC of the CLAS12 accounting for acceptance and smearing of the detector. Comparison of the PEPSI MC and the CLAS data for dihadron production shows very good agreement already at 6 GeV (See Figs.19 and 20).

Studies of other sources of systematics, related to physics background, including target fragmentation, semi-exclusive processes, exclusive vector meson contributions, and higher twist require the data of this measurement. A cut on the missing mass of the dihadron pairs will be used to suppress contamination from exclusive production.

For our estimate of the total systematic error, we have added the systematic errors from the various contributions in quadrature. The main sources of systematic errors

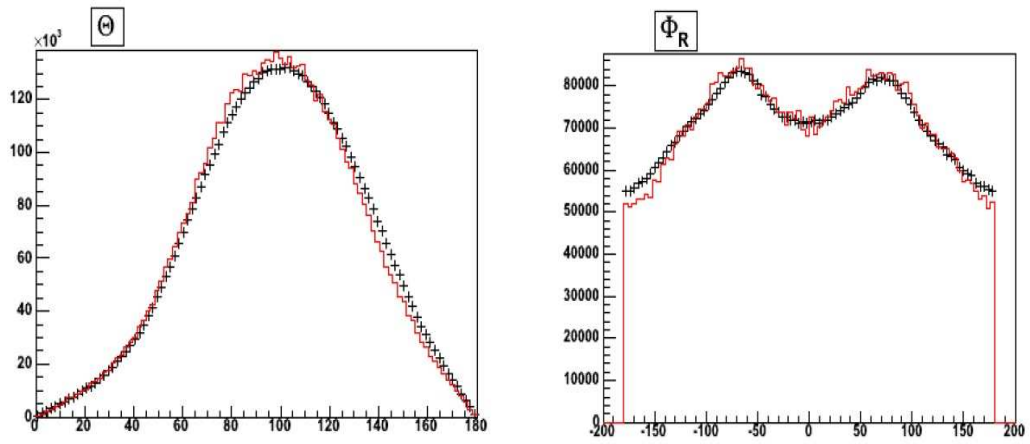


Figure 20: Comparison of angular distributions in $\theta$ (left) and $\phi_R$ (right) for charged pions using PEPSI+GEANT simulation of the CLAS eg1dvcs setup for dihadrons at 6 GeV with CLAS eg1dvcs data on pion pair electroproduction at 6 GeV.

in measurements of single spin asymmetries are listed in the Table 4. These errors are all scale errors, so they are proportional to the size of the measured asymmetry. Additional contributions to systematic error of measured asymmetries will come from uncertainties of unpolarized structure functions and dihadron FFs. We conservatively estimate the total relative systematic error on the proton SSAs to be sufficiently small (below $\sim$ 8% ) to make a very significant measurement.

For the $A_{UT}^{\sin\phi}$ SSA, statistical uncertainties are expected to dominate the total uncertainty.

| Error source | Systematic error (%) |
|---|---|
| D background | 4 |
| Target polarization $P_T$ | 4 |
| acceptance corrections | 5 |
| Al background contribution | 3 |
| Radiative corrections | 2 |
| Total | $\sim 8$ |

Table 4: Estimated contributions to the relative systematic uncertainty on $A_{UT}$ in SIDIS $\pi^+\pi^-$ pair production.

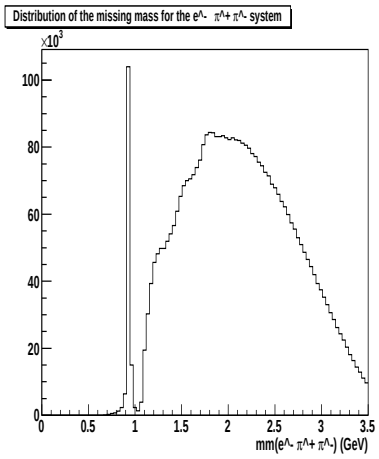


Figure 21: Missing mass distributions for pion pairs from PEPSI MC for $ehhX$ events.

## 5.3 Projected Results

Predicted statistical errors for polarized target asymmetries are based on the assumption of running 100 days on a HD-Ice target [82]. The number of days was chosen to achieve a statistical error that is not significantly larger than the systematical error at the highest $x$ and $M_{\pi\pi}$ points. The projections for electroproduction of dihadrons have been performed using the PEPSI (based on the PYTHIA) generator and the FASTMC processor of the CLAS12, accounting for the acceptance and smearing of the detector. The missing mass distributions for different hadron pair combinations are shown in Fig. 21. Various kinematic distributions for two hadron production are shown on Figs.22-25. A cut on the $x_F > 0$, ($x_F$ is the fraction of the longitudinal momentum in the center of mass frame) was used to separate particles in the target fragmentation region (TFR) and the current fragmentation region (CFR), respectively.

The kinematic region considered for these projections is the following: $Q^2 > 1$ GeV$^2$ (corresponding to $x > 0.05$), $W^2 > 4$ GeV$^2$, $0.10 < y < 0.85$ and $0.3 < z < 0.8$. A squared missing mass greater than 2 GeV$^2$ was also required. The projected results were obtained from a Monte Carlo simulation including a description of the CLAS12 geometry as well as detector acceptance and smearing effects. QED radiative effects were neglected since known, from previous studies, to be small. Here, a target polarization of 60% and a dilution factor of 1/3 were assumed.

Figure 26 shows the absolute error in all four dimensional bins of accessible phase space for transverse target spin asymmetry $A_{UT}$ on a proton target, corresponding to 100 days of data-taking with the HD-Ice target. For a significant measurement, we summed over a number of bins. The projected CLAS12 statistical precision on the $A_{UT}$ asymmetries for pion pairs is integrated over other variables bins is shown in Fig. 27. Error bands represent upper and lower limits of different model calculations

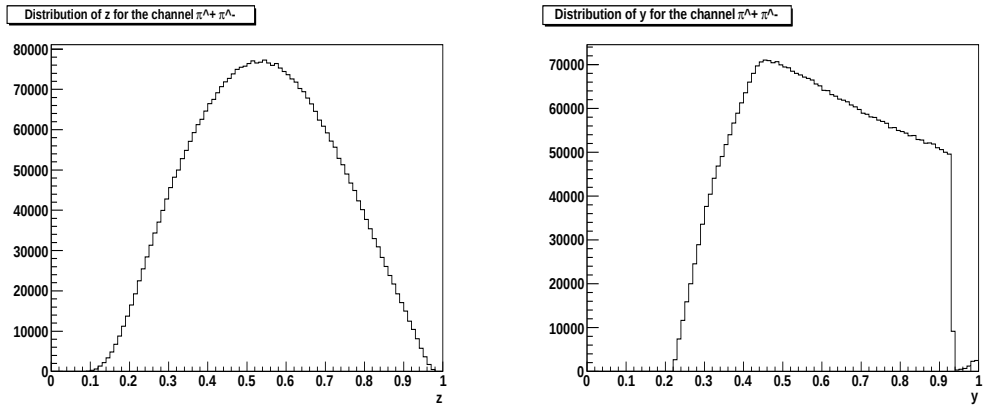


Figure 22: $z$ and $y$-distributions of pion pairs.

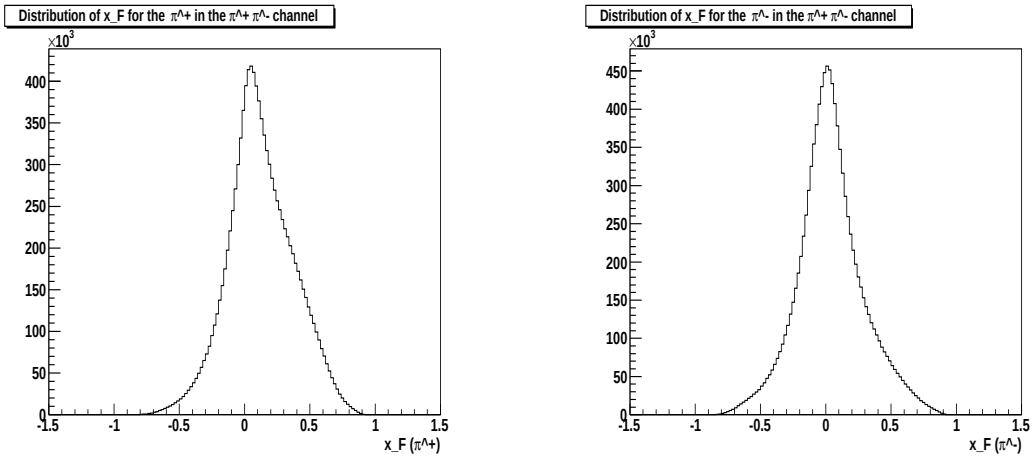


Figure 23: $x_F$-distributions of $\pi^+$ (left) and $\pi^-$ (right) of pion pairs.

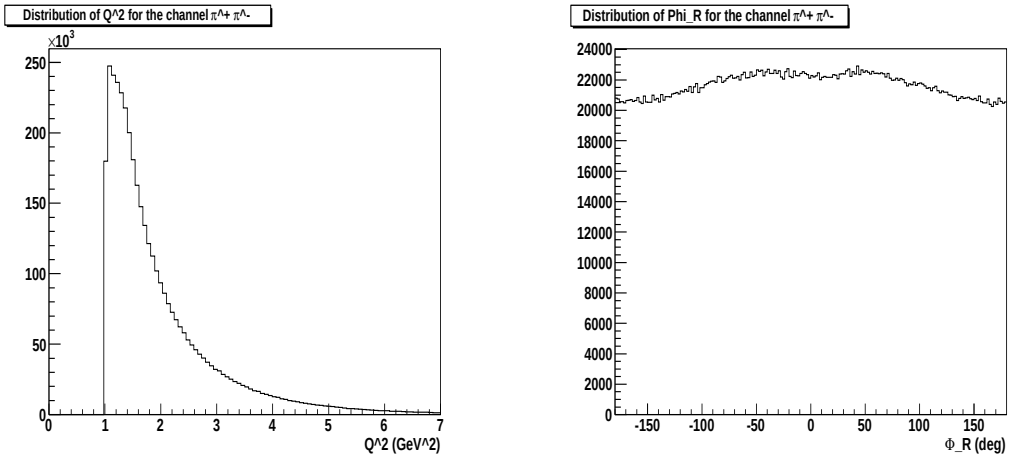


Figure 24: The $Q^2$-distribution of pion pairs (left) and the $\phi_R$-distribution of the pair (right).

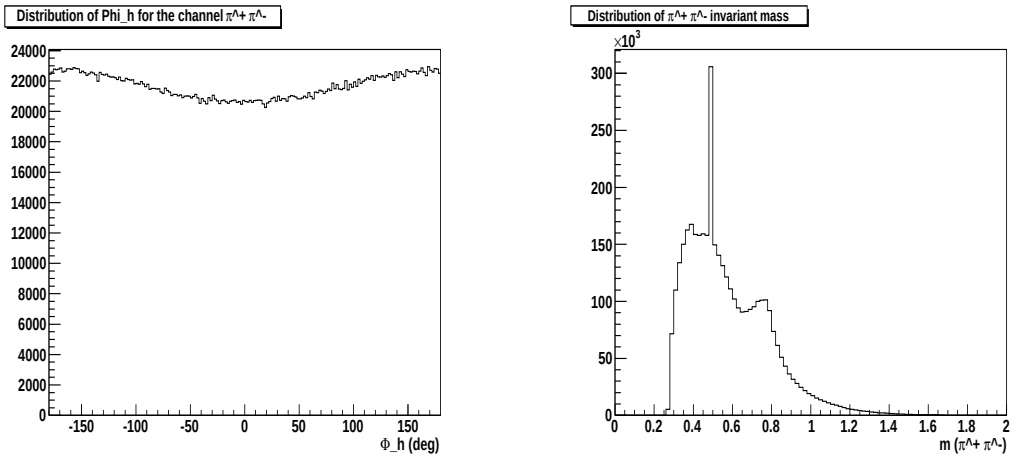


Figure 25: The $\phi_h$ distribution (left) and invariant mass $M_\pi\pi$ distributions (right) for pion pair SIDIS.

shown in Fig. 6.

# 6 Summary and Beam Time Request

We propose a study of the transversity parton distributions via measurements of pion pair electro-production in SIDIS in the hard scattering regime ($Q^2 > 1$ GeV$^2$, $W^2 > 4$ GeV$^2$), using an 11 GeV electron beam from the upgraded CEBAF facility and the CLAS12 detector.

We request 110 days of beam time with high polarization of electrons at 11 GeV and a transversely polarized hydrogen target (100 days of data-taking plus 10 days for calibration, empty target runs and supportive tests). We expect to improve substantially the statistical precision of the HERMES and COMPASS measurements for the hydrogen target. The comparison between the projected results for CLAS12 and the HERMES results, as extracted via DiFF [32, 73, 74] (Fig. 28) shows the remarkable improvement expected for CLAS12 in terms of statistical precision and kinematic coverage, especially in the valence region (intermediate-to-high $x$). For deuterium, the errors should be inflated by a factor of 4.5[4], taking into account its smaller polarization and greater dilution factor. The precision mapping of transverse SSA in the valence region is important to extract fundamental quantities like the tensor charge [58, 83], which can be compared to Lattice QCD calculations [84].

The large acceptance of the CLAS12 detector permits a simultaneous scan of various variables ($x_B$, $z$, $M_{\pi\pi}$and $Q^2$). The HD-Ice target provides a full kinematical coverage of measurements, in particular at large $Q^2$, providing a control over possible higher twist contributions. One of the important advantages of the HD-Ice target

[4]assuming an order of magnitude lower luminosity, the deuteron can stand

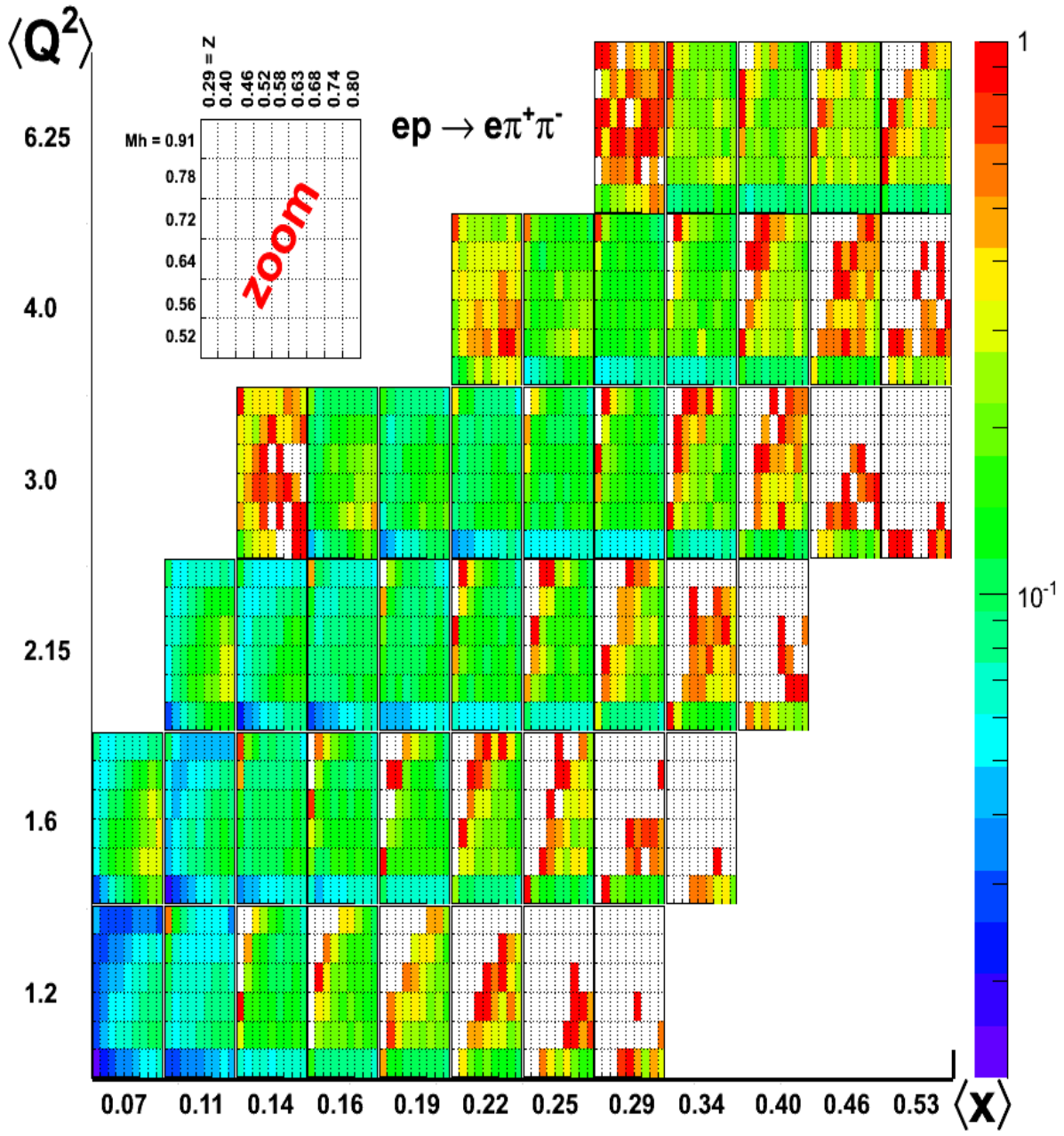


Figure 26: A 4D plot with errors (in color) with external squares corresponding to $x$ vs $Q^2$ and with internal squares corresponding to $z$ vs $M_h$.

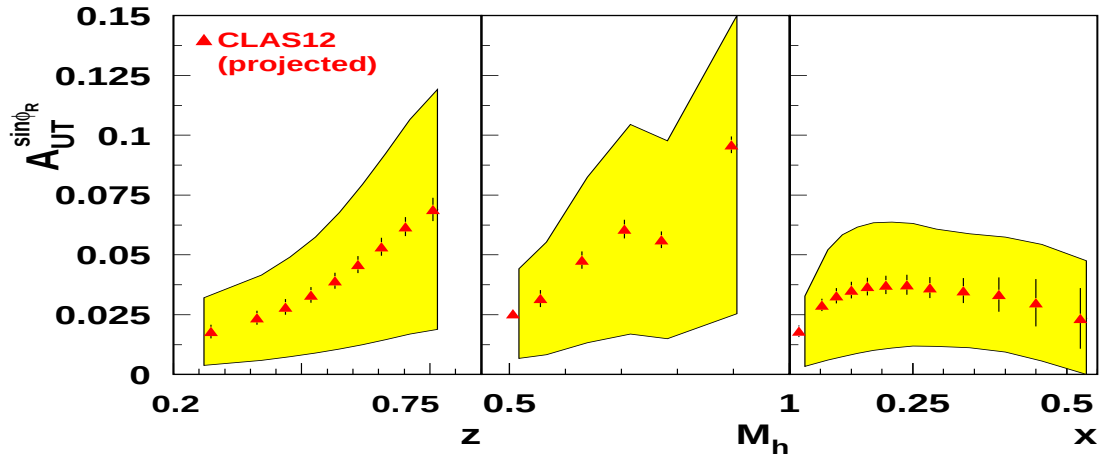


Figure 27: The projected statistical error for data on a hydrogen target (100 days of HD-Ice) for the target asymmetry $A_{UT}^{\sin\phi_R \sin\theta}$ in ($z$, $M_{\pi\pi}$, $x$). The band represent the spread in predictions for three different models for $h_1(x)$ from Fig. 6.

compared to nuclear targets ($NH_3$, $ND_3$) is its superior dilution factor, which is crucial for studies of transverse momentum dependences.

Analysis of already existing electroproduction data from CLAS with unpolarized and longitudinally polarized targets has shown that JLab 6 GeV data are consistent with the PYTHIA MC and proposed measurements are feasible.

### Beam Request

**We ask the PAC to award 110 days of beam time for a dedicated high statistics SIDIS experiment with a transversely polarized target.**

The measurement of the target SSA in hadron pair production off a transversely polarized proton would allow precision measurements of flavor contribution of the underlying transversity PDF.

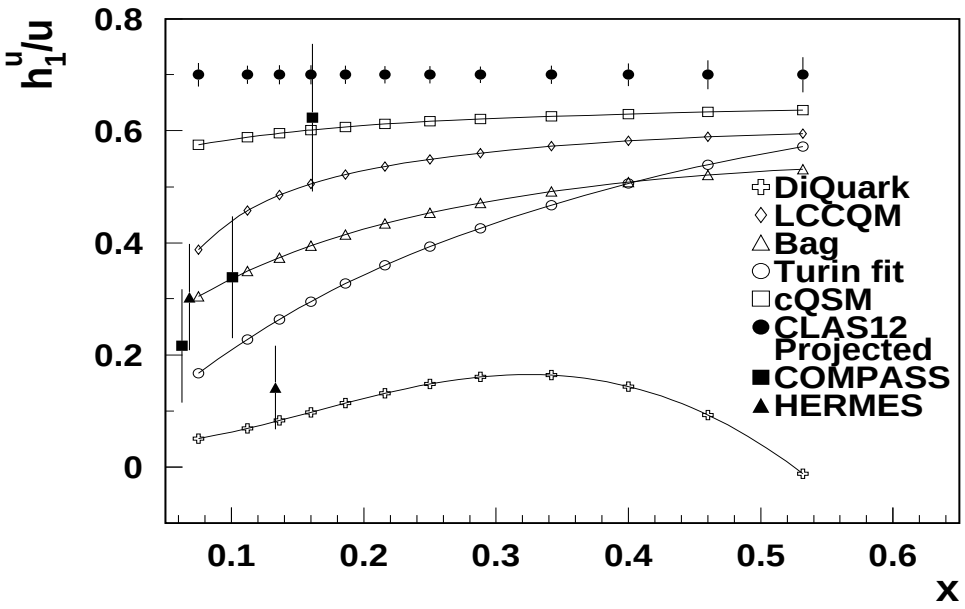


Figure 28: The projected statistical error for transversity (100 days of HD-Ice) as a function of $x$. The curves show different models for $h_1(x)$ from Fig. 6 as well as the extraction from HERMES and COMPASS from Fig. 8.

# References


[1] J.P. Ralston and D.E. Soper, Nucl. Phys. B152 (1979) 109.

[2] R.L. Jaffe and X.D. Ji, Phys. Rev. Lett. 67 (1991) 552.

[3] J. Cortes, B. Pire and J. Ralston, Z.Phys. C55 (1992) 409.

[4] X. Artru and M. Mekhfi, Z. Phys. C45 (1990) 669.

[5] M. Gockeler et al., (2006), hep-lat/0612032.

[6] V. Barone, A. Drago and P.G. Ratcliffe, Phys. Rept. 359 (2002) 1, hep-ph/0104283.

[7] J.C. Collins, Nucl. Phys. B396 (1993) 161, hep-ph/9208213.

[8] HERMES, A. Airapetian et al., Phys. Lett. B693 (2010) 11, 1006.4221.

[9] The COMPASS, M.G. Alekseev et al., Phys. Lett. B692 (2010) 240, 1005.5609.

[10] D. Boer, R. Jakob and P.J. Mulders, Nucl. Phys. B504 (1997) 345, hep-ph/9702281.

[11] Belle, K. Abe et al., Phys. Rev. Lett. 96 (2006) 232002, hep-ex/0507063.

[12] Belle, R. Seidl et al., Phys. Rev. D78 (2008) 032011, 0805.2975.

[13] M. Anselmino et al., (2007), hep-ph/0701006.

[14] J.C. Collins and D.E. Soper, Nucl. Phys. B193 (1981) 381.

[15] X. Ji, J. Ma and F. Yuan, Phys. Rev. D71 (2005) 034005, hep-ph/0404183.

[16] D. Boer, Nucl. Phys. B806 (2009) 23, 0804.2408.

[17] M. Anselmino, M. Boglione and S. Melis, (2012), 1204.1239.

[18] D. Boer et al., (2011), in preparation.

[19] S.M. Aybat and T.C. Rogers, Phys.Rev. D83 (2011) 114042, 1101.5057.

[20] J.C. Collins, D.E. Soper and G. Sterman, Adv. Ser. Direct. High Energy Phys. 5 (1988) 1, hep-ph/0409313.

[21] CTEQ, R. Brock et al., Rev. Mod. Phys. 67 (1995) 157.

[22] M. Radici, R. Jakob and A. Bianconi, Phys. Rev. D65 (2002) 074031, hep-ph/0110252.

[23] A.V. Efremov, L. Mankiewicz and N.A. Tornqvist, Phys. Lett. B284 (1992) 394.

[24] J.C. Collins and G.A. Ladinsky, (1994), hep-ph/9411444.

[25] R.L. Jaffe, X. Jin and J. Tang, Phys. Rev. Lett. 80 (1998) 1166, hep-ph/9709322.

[26] A. Bacchetta and M. Radici, Phys. Rev. D67 (2003) 094002, hep-ph/0212300.

[27] HERMES, A. Airapetian et al., JHEP 06 (2008) 017, 0803.2367.

[28] COMPASS Collaboration, C. Adolph et al., (2012), 1202.6150.

[29] BELLE Collaboration, A. Vossen et al., Phys.Rev.Lett. (2011), 1104.2425.

[30] X. Artru and J.C. Collins, Z. Phys. C69 (1996) 277, hep-ph/9504220.

[31] D. Boer, R. Jakob and M. Radici, Phys. Rev. D67 (2003) 094003, hep-ph/0302232.

[32] A. Bacchetta, A. Courtoy and M. Radici, (2011), 1104.3855.

[33] The Jefferson Lab Hall A Collaboration, X. Qian et al., Phys.Rev.Lett. 107 (2011) 072003, 1106.0363, 6 pages, 2 figures, 2 tables, published in PRL.

[34] PHENIX, R. Yang, AIP Conf.Proc. 1182 (2009) 569.

[35] E. Leader, A.V. Sidorov and D.B. Stamenov, Phys.Rev. D82 (2010) 114018, 1010.0574.

[36] A. Bacchetta et al., JHEP 02 (2007) 093, hep-ph/0611265.

[37] M. Diehl and S. Sapeta, Eur. Phys. J. C41 (2005) 515, hep-ph/0503023.

[38] A. Bacchetta et al., Phys. Rev. D70 (2004) 117504, hep-ph/0410050.

[39] J. Zhou and A. Metz, Phys. Rev. Lett. 106 (2011) 172001, hep-ph/1101.3273.

[40] A. Bacchetta and M. Radici, Phys. Rev. D69 (2004) 074026, hep-ph/0311173.

[41] A. Courtoy et al., (2012), 1202.0323.

[42] S. Gliske, PhD. thesis, http://www-hermes.desy.de/notes/pub/10-LIB/sgliske.10-003.sidis-vm.pdf.

[43] A. Bianconi et al., Phys. Rev. D62 (2000) 034009, hep-ph/9907488.

[44] A. Bacchetta and M. Radici, Phys. Rev. D74 (2006) 114007, hep-ph/0608037.

[45] A. Bacchetta et al., Phys. Rev. D79 (2009) 034029, 0812.0611.

[46] A. Casey, H.H. Matevosyan and A.W. Thomas, (2012), 1202.4036.

[47] X. Artru and J.C. Collins, Z. Phys. C69 (1996) 277, hep-ph/9504220.

[48] R.L. Jaffe and X. Ji, Nucl. Phys. B375 (1992) 527.

[49] R.L. Jaffe, (1996), hep-ph/9602236.

[50] A. Hayashigaki, Y. Kanazawa and Y. Koike, Phys. Rev. D56 (1997) 7350, hep-ph/9707208.

[51] S. Kumano and M. Miyama, Phys. Rev. D56 (1997) 2504, hep-ph/9706420.

[52] W. Vogelsang, Phys. Rev. D57 (1998) 1886, hep-ph/9706511.

[53] I.C. Cloet, W. Bentz and A.W. Thomas, Phys. Lett. B659 (2008) 214, 0708.3246.

[54] M. Wakamatsu, Phys. Lett. B653 (2007) 398, 0705.2917.

[55] H. He and X. Ji, Phys. Rev. D52 (1995) 2960, hep-ph/9412235.

[56] B. Pasquini, M. Pincetti and S. Boffi, Phys. Rev. D76 (2007) 034020, hep-ph/0612094.

[57] L.P. Gamberg and G.R. Goldstein, Phys. Rev. Lett. 87 (2001) 242001, hep-ph/0107176.

[58] M. Anselmino et al., Nucl. Phys. Proc. Suppl. 191 (2009) 98, 0812.4366.

[59] J. Soffer, Phys. Rev. Lett. 74 (1995) 1292, hep-ph/9409254.

[60] C. Bourrely, J. Soffer and O.V. Teryaev, Phys. Lett. B420 (1998) 375, hep-ph/9710224.

[61] P.V. Pobylitsa and M.V. Polyakov, Phys. Lett. B389 (1996) 350, hep-ph/9608434.

[62] B.Q. Ma, I. Schmidt and J. Soffer, Phys.Lett. B441 (1998) 461, hep-ph/9710247.

[63] R. Jakob, P.J. Mulders and J. Rodrigues, Nucl. Phys. A626 (1997) 937, hep-ph/9704335.

[64] J. Soffer, M. Stratmann and W. Vogelsang, Phys. Rev. D65 (2002) 114024, hep-ph/0204058.

[65] V.A. Korotkov, W.D. Nowak and K.A. Oganessyan, Eur. Phys. J. C18 (2001) 639, hep-ph/0002268.

[66] P. Schweitzer et al., Phys. Rev. D64 (2001) 034013, hep-ph/0101300.

[67] B. Pasquini, M. Pincetti and S. Boffi, Phys. Rev. D72 (2005) 094029, hep-ph/0510376.

[68] A. Bacchetta et al., (2008), hep-ph/0807.0323.

[69] C. Bourrely, F. Buccella and J. Soffer, (2010), 1008.5322.

[70] A.D. Martin et al., Eur. Phys. J. C63 (2009) 189, 0901.0002.

[71] D. de Florian, G. Navarro and R. Sassot, Phys.Rev. D71 (2005) 094018, hep-ph/0504155.

[72] A. Bacchetta et al., Eur. Phys. J. A45 (2010) 373, 1003.1328.

[73] M. Radici, (2011), 1111.3383.

[74] A. Courtoy, A. Bacchetta and M. Radici, (2012), in preparation.

[75] Jefferson Lab Hall B, H. Avakian et al., PAC38 Proposal .

[76] W.K. Brooks and H. Hakobyan, Nucl. Phys. A830 (2009) 361c, 0907.4606.

[77] HERMES, A. Airapetian et al., Phys. Rev. Lett. 103 (2009) 152002, 0906.3918.

[78] CLAS, A. Sandorfi et al., CLAS proposal E06-101 (2006).

[79] A. Caracappa and C. Thorn, AIP Conf. Proc. 675 (2003) 867.

[80] C. Thorn and A. Caracappa, AIP Conf. Proc. (2007) (in press).

[81] Jefferson Lab Hall A, M.K. Jones et al., Phys. Rev. Lett. 84 (2000) 1398, nucl-ex/9910005.

[82] Jefferson Lab Hall B, H. Avakian et al., PAC38 Proposal (PR12-11-111) .

[83] M. Wakamatsu, Phys. Rev. D79 (2009) 0140338, 0811.4196.

[84] M. Goeckeler et al., Phys. Lett. B627 (2005) 113, 0507001.